Acta Pharmaceutica Sinica B xxxx;xxx(xxx):xxx

Chinese Pharmaceutical Association
Institute of Materia Medica, Chinese Academy of Medical Sciences

Acta Pharmaceutica Sinica B

www.elsevier.com/locate/apsb
www.sciencedirect.com

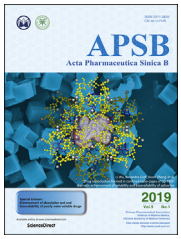

ORIGINAL ARTICLE

Ginsenoside modified lipid-coated perfluorocarbon nanodroplets: A novel approach to reduce complement protein adsorption and prolong *in vivo* circulation

Jie Zhou[a,b], Binyang Gao[a,b], Huan Zhang[a,b], Rui Yang[a,b], Jianbo Huang[a,b], Xin Li[c], Yi Zhong[c], Yan Wang[d], Xiaoxia Zhu[a,b], Yan Luo[a,b,*], Feng Yan[a,b,*]

[a]*Ultrasound Department of West China Hospital, Sichuan University, Chengdu 610041, China*
[b]*Laboratory of Ultrasound Imaging of West China Hospital, Sichuan University, Chengdu 610041, China*
[c]*West China Washington Mitochondria and Metabolism Research Center, West China Hospital, Sichuan University, Chengdu 610041, China*
[d]*Research Core Facilities of West China Hospital, Sichuan University, Chengdu 610041, China*

Received 7 August 2023; received in revised form 31 October 2023; accepted 3 November 2023

KEY WORDS

Lipid-coated perfluorocarbon nanodroplets;
Protein corona;
Complement C3;
Phagocytosis;
Ginsenoside lipid-coated perfluorocarbon nanodroplets;
Innate immune system;
Complement system;
Mononuclear phagocytic system

Abstract Lipid-coated perfluorocarbon nanodroplets (lp-NDs) hold great promise in bio-medicine as vehicles for drug delivery, molecular imaging and vaccine agents. However, their clinical utility is restricted by limited targeted accumulation, attributed to the innate immune system (IIS), which acts as the initial defense mechanism in humans. This study aimed to optimize lp-ND formulations to minimize non-specific clearance by the IIS. Ginsenosides (Gs), the principal components of *Panax ginseng*, possessing complement inhibition ability, structural similarity to cholesterol, and comparable fat solubility to phospholipids, were used as promising candidate IIS inhibitors. Two different types of ginsenoside-based lp-NDs (Gs lp-NDs) were created, and their efficacy in reducing IIS recognition was examined. The Gs lp-NDs were observed to inhibit the adsorption of C3 in the protein corona (PC) and the generation of SC5b-9. Adding Gs to lp-NDs reduced complement adsorption and phagocytosis, resulting in a longer blood circulation time *in vivo* compared to lp-NDs that did not contain Gs. These results suggest that Gs can act as anti-complement and anti-phagocytosis adjuvants, potentially reducing non-specific clearance by the IIS and improving lifespan.

*Corresponding authors.
E-mail addresses: yan_feng@scu.edu.cn (Feng Yan), luoyanddoc@163.com (Yan Luo).

Peer review under the responsibility of Chinese Pharmaceutical Association and Institute of Materia Medica, Chinese Academy of Medical Sciences.

https://doi.org/10.1016/j.apsb.2023.11.016

Please cite this article as: Zhou Jie et al., Ginsenoside modified lipid-coated perfluorocarbon nanodroplets: A novel approach to reduce complement protein adsorption and prolong *in vivo* circulation, Acta Pharmaceutica Sinica B, https://doi.org/10.1016/j.apsb.2023.11.016

1. Introduction

In the past twenty years, lipid-coated perfluorocarbon nanodroplets (lp-NDs) have been extensively studied as effective contrast agents in diagnostic imaging and therapy[1]. These lp-NDs, generated from phospholipids structurally similar to those located in the cell membrane, are biocompatible and biodegradable carriers capable of encapsulating fat-soluble drugs and oxygen in the perfluorocarbon (PFC) core. The liquid PFC with high oxygen solubility enables them to act as blood substitutes and transport oxygen[2,3]. Additionally, they can convert into gaseous echogenic microbubbles when activated by an external stimulus[4].

While intense research efforts have focused on the clinical translation of lp-NDs, their *in vivo* application encounters substantial challenges. A significant concern is the non-specific removal of these foreign substances by the innate immune system (IIS). The IIS, which includes the mononuclear phagocytic system (MPS) and the complement system, plays essential parts in protecting the body against viruses, bacteria and micro-/nanoparticles[5]. After being administered intravenously, nanoparticles (NPs) quickly become coated by blood proteins, forming the "protein corona (PC)". This process, known as opsonization, involves active complement fragments (like C3b/iC3b), immunoglobulins, and other opsonins that coat the surface of the NPs and trigger phagocytotic activity[6]. Ultimately, similar to other NPs, lp-NDs are considered foreign objects and are eliminated promptly from the bloodstream[7]. Improved understanding of the mechanisms by which lp-NDs interact with opsonins and macrophages is therefore crucial for reducing non-specific clearance and improving their delivery efficacy.

Various innovative methods have been established to prevent the indiscriminate clearance of NPs. These involve regulating their physicochemical features, including surface charge, size, hydrophilicity, and functionality[8,9]. The grafting of polyethylene glycol (PEG) is a universally used technique in NPs, which involves attaching a hydrophilic and flexible polymer to their surface to reduce non-specific uptake[10–12]. Examples of PEG used include Genexol-PM, Onivyde, Active Ingredient, Lipoplatin, and NK105, with the former three consisting of Active Ingredient, Active Ingredient, and Active Ingredient, respectively, in PEGylated liposomes or a polymeric micelle; while the latter two are in late-stage clinical development[13,14]. However, PEG modifications could enhance the immunogenicity of NPs, which might induce an anti-PEG antibody reaction upon frequent intravenous administration of PEGylated NPs. This re-action could hasten blood clearance and potentially cause acute hypersensitivity[15].

The complement system of IIS, made up of more than thirty proteins, works through a complex cascade mechanism that is triggered *via* three pathways: the classical pathway (CP), activated by complexes of antigen−antibody; the alternative pathway (AP), activated unprompted by complement components attaching to pathogen surfaces; and the lectin pathway (LP), where mannan-binding lectin or ficolin interact with mannose-containing carbohydrates on bacterial or viral surfaces[16]. The three complement pathways converge at C3 and share a common final pathway, underscoring the pivotal significance of the C3 in the complement system[17]. Inhibition of complement activation presents an uncommon but efficient strategy to suppress opsonophagocytosis.

Based on the molecular mechanisms underlying lp-NDs' non-specific clearance, introduction of surface modifications that reduce IIS recognition is currently a significant focus of research. Ginseng, the valuable root of *Panax ginseng* C.A. Meyer (family Araliaceae), is a highly regarded herbal medicine that finds extensive use in Asia, notably in China, Japan, and Korea[18]. The beneficial effects of ginseng are thought to be its primary active components, the dammarane-type triterpene saponins known as ginsenosides (Gs). The Gs possess an aglycone featuring a distinctive dammarane framework, with a skeleton portion that closely resembles that of cholesterol[19,20]. Prior research has demonstrated that Gs displays an anti-complement effect[21], and may stabilize mixed phospholipid-ginsenoside membranes, akin to cholesterol[22,23].

The study aimed to identify the PC components on lp-ND surface and examine how complement proteins in the corona affect non-specific clearance by IIS. Furthermore, we aimed to optimize preparations of ginsenoside lp-NDs (Gs lp-NDs), and examined the anti-complement and anti-phagocytosis activities of lp-NDs formulated with Gs as well as their biosafety, biocompatibility, and bio-metabolism properties.

2. Materials and methods

2.1. Materials

Lipid agents used for lp-NDs synthesis, including 1,2-dipalmitoyl-*sn*-glycero-3-phosphocholine (DPPC) (catalog no. T0343) and 1,2-distearyl-*sn*-glycero-3-phosphoethanolamine-*N*-[methoxy (polyethylene glycol)2000] (DSPE-mPEG2000) (catalog no. B80580) were purchased fron AVT Pharmaceutical Tech Co. (Shanghai, China). The core is filled with phase-transition material perfluorohexane (C_6F_{14}) (Matrix Scientific, catalog no. U10M, Colombia, SC, USA). Recombinant Active Ingredient (Boatman Biotech, catalog no. BRHD12A, Shanghai, China) was employed as an anticoagulant agent. Gs Rd (catalog no. PU0561-0025), Rh2 (cat-alog no. PS0956-0025), and Re (catalog no. PU0336-0025) were purchased from Push Biotechnology (Chengdu, China). Mouse anti-human C1q antibody (catalog no. ab71940) and mouse anti-human properdin antibody (catalog no. ab58984) were purchased from Abcam (Cambridge, MA, USA). Ethylenediaminetetraacetic acid (EDTA) (catalog no. R003464) and ethylene glycol tetraacetic acid (EGTA) (catalog no. R016727) were purchased from Rhawn Chemical Technology (Shanghai, China). Fluorescent probes included 1,1′-dioctadecyl-3,3,3′,3′-tetramethylindocarbocyanine perchlorate (DiI) (Beyotime Biotechnology, catalog no. C1036, Shanghai, China), LysoTracker (Beyotime Biotechnology, catalog no. C1047S) and Hoechst (Beyotime Biotechnology, catalog no. C1011). Magnesium chloride ($MgCI_2$) (catalog no. M4880) was obtained from Sigma (St. Louis, MO, USA). Phosphate buffer saline (PBS) (catalog no. P1020) and 10% Sodium dodecyl sulfate (SDS)

Please cite this article as: Zhou Jie et al., Ginsenoside modified lipid-coated perfluorocarbon nanodroplets: A novel approach to reduce complement protein adsorption and prolong *in vivo* circulation, Acta Pharmaceutica Sinica B, https://doi.org/10.1016/j.apsb.2023.11.016

(catalog no. S1010) were obtained from Solarbio Science & Technology (Beijing, China).

The experimental protocol was reviewed and approved by the Ethics Committee of West China Hospital of Sichuan University (Ethics approval number: 2021889).

2.2. Preparation and characterization of lp-NDs

We employed a thin-film hydration technique as described below to produce lp-NDs. The formulas of lp-NDs and Gs lp-NDs are provided in Table 1. In brief, lp-NDs consisted of DPPC and DSPE-mPEG2000 in a molar ratio of 95:5, while Gs lp-NDs incorporated varying Gs (25%, 50% and 75% molar ratio, respectively), DPPC and DSPE-mPEG2000. All lipids and Gs were homogeneously mixed in chloroform (shell material quality/chloroform volume, 5 mg/mL, Keshi, Chengdu, China). The shell solution was concentrated by rotary evaporation (Shanghai Yarong Biochemical Instrument Factory, RE2000B, Shanghai, China) at 50 °C overnight to produce the shell membrane, which was then dispersed using an ultrasonic cleaner (Scientz Biotechnology, SCIENTZ-IID, Ningbo, China) with sterile saline (shell membrane quality/saline volume, 0.2 mg/mL) at 50 °C. After the solution was cooled, 5 mL of the suspension was mixed with 1 mL of C_6F_{14} on an ice bath for 5 min. The mixture was transformed into particles by sonication for 5 min at 300 W (50% duty cycle) using a ultrasonic oscillator (Scientz Biotechnology, SCIENTZ-IID). The particle suspension was filtered using a hand extruder (Genizer, HandExtruder-1ml, Los Angeles, CA, USA) equipped with a polycarbonate membrane filter (Genizer, 19.05 mm in diameter and 0.4 μm pore size). The resulting lp-NDs were stored at 4 °C and its morphology was observed by an electron microscope (FEI Company, Tecnai G2 F20 S-TWIN, Hillsboro, OR, USA). The concentration of lp-NDs was quantified using the nanoparticle tracking instrument (Particle Metrix, ZetaView, Meerbusch, Germany). The size, polydispersity index (PDI), and zeta potential (ZP) of all lp-NDs were assessed utilizing the Brookhaven analyzer (Brookhaven Instruments Corporation, NanoBrook 90plus PALS, Holtsville, NY, USA).

Table 1 The composition and the nomenclature of the different lp-NDs.

Nomenclature	Composition (molar ratio)
Lp-NDs/C lp-NDs	95% DPPC+5% DSPE-mPEG2000
Non-PEG lp-NDs	100% DPPC
75% Rd lp-NDs	75% Rd+20% DPPC+5% DSPE-mPEG2000
50% Rd lp-NDs	50% Rd+45% DPPC+5% DSPE-mPEG2000
25% Rd lp-NDs	25% Rd+70% DPPC+5% DSPE-mPEG2000
75% Rh2 lp-NDs	75% Rh2+20% DPPC+5% DSPE-mPEG2000
50% Rh2 lp-NDs	50% Rh2+45% DPPC+5% DSPE-mPEG2000
25% Rh2 lp-NDs	25% Rh2+70% DPPC+5% DSPE-mPEG2000

DPPS, diphenylbis(4-(pyridin-3-yl)phenyl)silane; DPPC, 1,2-dihexadecanoyl-*rac*-glycero-3-phosphocholine; DSPE-mPEG2000, *N*-(carbonyl-methoxypolyethylene glycol 2000)-1,2-distearoyl-*sn*-glycerol-3-phosphoethanolamine, sodium salt.

2.3. Fourier transform infrared spectroscopy (FTIR) of Gs lp-NDs

The Gs in Gs lp-NDs was confirmed *via* FTIR spectroscopy. Gs Rd and Rh2 contain double bonds (C=C) in their chemical structure (Fig. 1A). An infrared spectrometer (Thermo Nicolet Corporation, Nicolet IS10, Madison, GA, USA) was used for FTIR spectroscopy in the KBr pellet mode. FTIR spectra were acquired within the 400−4000 cm^{-1} range.

2.4. Assessment of Gs encapsulation in Gs lp-NDs

Ultra-performance liquid chromatography (UPLC) coupled with the AB Sciex 5500 Qtrap system, a hybrid triple quadrupole/linear ion trap mass spectrometry (MS) (AB SCIEX, Redwood City, CA, USA) was utilized to quantify the Gs in Gs lp-NDs. Briefly, 5 mg of Gs was diluted in 1 mL of chloroform as the mixed stock standard solution. Working solutions were prepared from the stock standard *via* dilution with methanol. The Gs Re was used as an internal reference solution (working concentration 12 μg/mL). Gs lp-NDs (1×10^{12} particles/mL; 200 μL) were mixed with 50 μL of the internal reference solution and 100 μL of acetonitrile. The mixture was vortexed for 30 min at 4 °C to promote demulsification. Next, the demulsified solution was dried using a soft nitrogen flow at a temperature of 37 °C. Residues were dissolved in a solution of 50% methanol and 50% water (*v*/*v*) and then subjected to vortex mixing for 30 min followed by centrifugation at 4 °C and 100,000 ×*g* for 20 min. Ultimately, 5 μL of supernatant was used for analysis. A Phenomenex C18 column (50 mm × 22.1 mm, 1.7 μm) was utilized for separation at 35 °C with the mobile phase being a mixture of 0.05% ammonia water (A) and acetonitrile (B). The following gradient elution program was employed: from 0 to 4 min, the eluent B concentration was increased from 10% to 90%; from 4 to 5 min, the eluent B concentration was kept at 90%; from 5 to 5.01 min, the eluent B concentration was decreased from 90% to 10%; from 5.01 to 6 min, the eluent B concentration was maintained at 10%. Flow rate was maintained at 0.45 mL/min. Ionization of Gs Rd and Re was performed using an electrospray negative ion source (ESR^-). An electrospray positive ion source (ESR^+) was utilized for ionization of Gs Rh2, followed by detection in the multiple reaction monitoring mode. Table 2 summarizes the mass spectrometry parameters such as molecular mass, precursor ions, fragment ions, declustering potential and collision energy. The calculation of encapsulation efficiency (EE) was based on the subsequent Eq. (1)

$$EE\,(\%) = Encapsulated_{Gs}/Total_{Gs} \times 100 \quad (1)$$

2.5. PC preparation

Experimental conditions (incubation time and temperature, elution method) were selected according to previous reports[24,25]. Whole human blood from healthy donor was collected into Active Ingredient tubes (containing 20 antithrombin units/mL). To create Lp-ND-protein complexes, lp-NDs (1×10^{12} particles/mL) were com-bined with Active Ingredient anticoagulated plasma (1:3, *v*/*v*; in the sub-sequent content, if no explicit specifications, 'plasma' refers to Active Ingredient-anticoagulated plasma), and incubated at 37 °C for 1 h. The mixture obtained was centrifuged at 100,000×*g* for

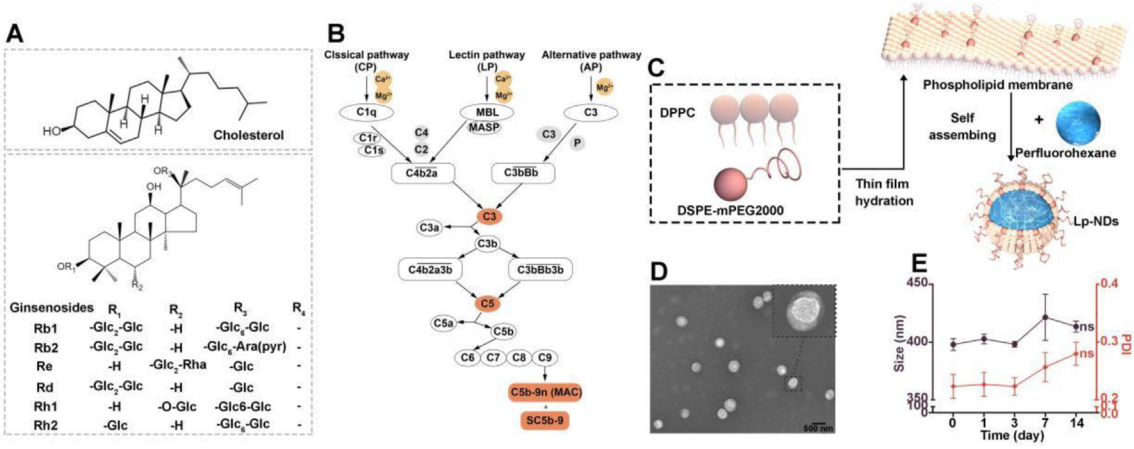

Figure 1 (A) Molecular structural formulae of cholesterol and ginsenosides. (B) Activation pathways of the complement system: proteins and dependent ions. (C) Schematic diagram of lp-ND preparation. (D) Transmission electron microscopy images of lp-NDs. Scale bar = 500 nm. (E) Changes in size and polydispersity index of lp-NDs stored at 4 °C in 14 days. Data are presented as mean ± SD (n = 3), ns, not significant.

15 min to isolate the complexes. The complexes formed were subjected to three wash cycles with phosphate buffered saline (PBS) to eliminate any unbound protein. Then, the lp-ND-protein complexes were incubated with 2% sodium dodecyl sulfate (SDS) in PBS for 1 h at room temperature to elute the PC, followed by ultracentrifugation at 1000×g for 10 min at room temperature.

2.6. *Analysis of binding proteins of lp-NDs*

Label-free liquid chromatography−mass spectrometry (LC−MS) analysis was conducted on plasma proteins attached to lp-NDs to determine the PC constituents. Enzymatic peptide segments were cleaned and desalted before MS analysis using a C18 Stage Tip column. A high-performance liquid chromatography system was used to introduce the PC solution into a C18 reverse phase column, and the peptides were examined with a Fusion Lumos Tribird mass spectrometer (Thermo Fisher Scientific, Wilmington, MA, USA). The MaxQuant software (Max Planck Institute of Biochemistry, Version1.6.2.6, https://maxquant.org/) and the "Wu Kong" platform (https://www.omicsolution.com/wkomics/main/) were used to scrutinize the MS data.

2.7. *Enzyme-linked immunosorbent assay (ELISA)*

The activation of complement by lp-NDs in the fluid phase was assessed by ELISA, which included quantification of C3 in the PC and SC5b-9 in Active Ingredient plasma.

2.7.1. *C3*

The ELISA kit (Abcam, catalog no. ab108822) was used to quantify the C3 concentration in PC, following the manufacturer's instructions.

2.7.2. *SC5b-9*

The SC5b-9 levels in human plasma and rat plasma were determined using ELISA kits specific for humans (MicroVue SC5b-9 Plus EIA, Quidel Corporation, San Diego, CA, USA) and rats (Hycult Biotech, HK106-01, Uden, Netherlands), respectively, following the manufacturer's instructions.

2.8. *Analysis of the complement activation pathway*

Complement activation by both the CP and the LP are Ca^{2+} and Mg^{2+} ion-dependent, whereas that by the AP requires only Mg^{2+} (Fig. 1B). To distinguish the pathway of complement activation, inhibitor of different pathways were added to plasma prior to the experiment, these included: EDTA (10 mmol/L), which inhibits all three pathways; EGTA/Mg^{2+} (10 mmol/L EGTA and 10 mmol/L $MgCl_2$), which specifically inhibits Ca^{2+} sensitive pathways; anti-C1q antibody (1:50 dilution), which inhibits the CP; anti-properdin (anti-P) antibody (1:500 dilution), which inhibits the AP; and 1 × PBS for control group. All inhibitors were added to plasma 30 min prior to the experiment and incubated at 37 °C. Next, lp-NDs (1 × 10^{12} particles/mL) were added to plasma (1:3 v/v) and incubated at 37 °C for 1 h. Samples were processed using the above C3 and SC5b-9 ELISA protocols.

2.9. In vitro *cellular uptake*

In advance, the necessary uptake materials were prepared. Specifically, all lp-NDs were prestained with the red DiI fluorescent lipophilic dye (5 μmol/L). Plasma were pre-incubated with EDTA (10 mmol/L) to impede complement activation. Subsequently, 1 × 10^{12} particles/mL of DiI-labeled lp-NDs were combined with EDTA plasma at a ratio of 1:3 v/v and incubated at 37 °C for 1 h. This process led to the formation of lp-NDs@PC [C-],

Table 2 Analytical parameters of UPLC−MS analysis of ginsenosides.

Ginsenoside	Q1 (m/z)	Q3 (m/z)	Declustering potential (eV)	Collision energy (eV)
Rd (ESR-)	945.8	783.2/621.5	−260	−50/−57
Rh2 (ESR+)	623.5	587.3/407.5	20	15/124
Re (ESR-)[a]	945.8	475.4/637.4	−216/−216	−66/−55

[a]Internal reference.

Please cite this article as: Zhou Jie et al., Ginsenoside modified lipid-coated perfluorocarbon nanodroplets: A novel approach to reduce complement protein adsorption and prolong *in vivo* circulation, Acta Pharmaceutica Sinica B, https://doi.org/10.1016/j.apsb.2023.11.016

characterized by lp-NDs with a protein corona lacking complement components. Simultaneously, DiI-labeled lp-NDs were mixed with untreated plasma using comparable procedures to prepare lp-NDs encapsulating complete complement components in their PC, referred to as lp-NDs@PC [C+]. As the control, lp-NDs were exposed to PBS, denoted as bare lp-NDs.

The Thp-1 (CellCook, catalog no. CC1904, Guangzhou, China) and NCI−H1299 (CellCook, catalog no. CC0203) cell lines were cultured in complete medium which was consist of RPMI 1640 medium (Gibco, Thermo Fisher Scientific, catalog no. 11875101) supplemented with 10% fetal calf serum (Gibco, Thermo Fisher Scientific, catalog no. 10100−147, Waltham, MA, USA) and Active Ingredient-Active Ingredient 10,000 units/mL (Gibco, Thermo Fisher Scientific, catalog no. 15140122), at 37 °C in a 95% air and 5% CO_2 humidified incubator. Additionally, Thp-1 cells were treated with 100 nmol/L phorbol myristate acetate (PMA) (Sigma, catalog no. P1585) for 48 h to induce differentiation before phagocytosis experimentation.

Peripheral blood mononuclear cells (PBMCs) were isolated from healthy donors' peripheral blood using a density gradient separation method, followed by subsequent purification through an adhesion-based method. Specifically, PBMCs were obtained from EDTA anticoagulated blood using human lymphocyte separation medium (Solarbio Science & Technology, catalog no. P8610). To obtain monocyte-derived macrophages, obtained PBMCs were cultured in complete medium at 37 °C in a 5% CO_2 cell incubator for a duration of 2 h. Non-adherent cells were subsequently eliminated, while adherent cells were gently washed twice with warm sterile PBS. The adherent cells were then cultivated in a complete medium supplemented with human granulocyte-macrophage colony-stimulating factor (GM-CSF) (PeproTech, catalog no. 300−23, Rocky Hill, CT, USA) at a concentration of 50 ng/mL. Every two days, half of the medium was renewed. Following a culture period of 5−7 days, the adherent cells differentiated into mature macrophages. In order to elicit polarization towards the M1 phenotype and procure fully mature peripheral blood macrophages (PBMs), the mature macrophages were subjected to stimulation with human lipopolysaccharide (LPS) (Sigma, catalog no. L4391) at a concentration of 50 ng/mL and human Active Ingredient-gamma (IFN-γ) (PeproTech, catalog no. 300−02) at a concentration of 20 ng/mL for a duration of 24 h.

To examine the impact of complement on phagocytosis, cellular uptake experiment was performed. The cells were incubated with DiI-labeled C lp-NDs, lp-NDs@PC [C-] and lp-NDs@PC [C+] at a concentration of 1×10^9 particles/mL, at room temperature for 1 h. Quantitative analysis was performed using flow cytometry (BD Biosciences, FACS Calibur, San Jose, CA, USA). In parallel, the cells were stained with the nuclear dye Hoechst (blue) for nuclear visualization and lysosome dye LysoTracker (green) for intracellular localization. Subsequently, imaging was performed using a fluorescent confocal laser scanning microscope (CLSM) (A1R-MP, Nikon Corporation, Tokyo, Japan). Quantification of the degree of co-localization between the two fluorescent dyes was achieved by colour scatter plots and calculation of the Pearson's correlation coefficient (PCC). Line-scan intensity curves obtained from single cell images using the Plot Profile plug-in of Fiji software (National Institutes of Health, version 1.53t, Bethesda, MD, USA).

2.10. Assay of anti-complement activity of Gs Rd and Rh2 monomers against the CP

The assay based on the complement fixation test was conducted in keeping with a reported protocol[26]. Sheep red blood cells (SRBCs) (Bersee, catalog no. RCB001, Beijing, China) were incubated with rabbit anti-sheep erythrocyte antibody (1:1000) (Bersee, catalog no. BM351Y) in GVB^{++} buffer (Sigma, catalog no. G6514, containing 141 mmol/L NaCl, 0.5 mmol/L $MgCI_2$, 0.15 mmol/L calcium chloride, 0.1% gelatin, 3.1 mmol/L barbituric acid and 1.8 mmol/L sodium barbital, pH 7.3−7.4) to prepare sensitized erythrocytes (SEs). Gs Rd and Rh2 were dissolved in dimethyl sulfoxide (DMSO) (Solarbio Science & Technology, catalog no. D8371) at a concentration of 2 mg/mL, and then further diluted with GVB^{++}. One to thirty dilution of guinea pig serum (Bersee, catalog no. BM361Y) was selected for submaximal hemolysis (the system reached 100% hemolysis). Detailed procedures and results obtained with this dilution ratio are provided in Supporting Information Section S1 and Fig. S1. Varying concentrations of Gs were combined with guinea pig serum and incubated for 10 min at 37 °C. Afterward, SEs were introduced and incubated at 37 °C for 30 min. The assay controls were subjected to the conditions listed in Table 3. After centrifugation at 4 °C and 1000 *g*, the values of optical density (OD) were measured at a wavelength of 405 nm. Anti-complement activity was expressed as hemolysis inhibition rate according to Eqs. (2)−(4):

$$\text{Hemolysis rate}_{\text{Gs}}\,(\%) = (\text{OD}_{\text{Gs test}} - \text{OD}_{\text{Gs control}}) \,/\, (\text{OD}_{\text{100\% lysis}} - \text{OD}_{\text{Gs control}}) \times 100 \quad (2)$$

$$\text{Hemolysis rate}_{\text{complement}}\,(\%) = \text{OD}_{\text{Complement}} / \text{OD}_{\text{100\% lysis}} \times 100 \quad (3)$$

$$\text{Hemolysis inhibition rate}\,(\%) = 1 - (\text{Hemolysis rate}_{\text{Gs}} \,/\, \text{Hemolysis rate}_{\text{Complemt}}) \times 100 \quad (4)$$

Table 3 The volume of components added in anti-complement assay of the classical pathway (μL).

Group	Gs test	Gs control	Complement	100% lysis
GVB^{++}	−	400	200	−
Serum of guinea pig	200	−	200	−
Gs solution	200	200	−	−
Rabbit anti-sheep erythrocyte antibody	100	−	100	−
2% SRBC	100	−	100	100
Ultrapure water	−	−	−	500

GVB^{++} buffer (141 mmol/L NaCI, 0.5 mmol/L MgCI2, 0.15 mmol/L calcium chloride, 0.1% gelatin, 3.1 mmol/L barbituric acid and 1.8 mmol/L sodium barbital, pH 7.3−7.4); Gs, ginsenoside; SRBC, sheep red blood cells; −, not applicable.

Please cite this article as: Zhou Jie et al., Ginsenoside modified lipid-coated perfluorocarbon nanodroplets: A novel approach to reduce complement protein adsorption and prolong *in vivo* circulation, Acta Pharmaceutica Sinica B, https://doi.org/10.1016/j.apsb.2023.11.016

2.11. Assay of anti-complement activity of Gs Rd and Rh2 monomers against the AP

Klerx's method was used to analyze the anti-complement activity *via* AP[27]. Stock solution of Gs Rd and Rh2 was diluted with GVB-Mg-EGTA (GVB^{++} buffer supplemented with 2 mmol/L $MgCl_2$, and 8 mmol/L EGTA). One to fifteen dilution of human serum was selected for submaximal hemolysis. The detailed procedures and results obtained with the selected dilution ratio are provided in Supporting Information section S2 and Fig. S2. The samples were mixed with human serum and incubated at 37 °C for 10 min, followed by the addition of 0.5% rabbit erythrocytes (RERs, Bersee, catalog no. RCB003) and further incubation at 37 °C for 30 min. Identical conditions were used for different assay controls (as specified in Table 4). OD values were measured at 405 nm after centrifugation (4 °C, 1000×*g*). Anti-complement activity was expressed as hemolysis inhibition rate according to the above Eq. (2−4).

2.12. Assay of the inhibitory effects of Gs Rd and Rh2 lp-NDs on the complement system

C lp-NDs, 25% Rd lp-NDs, and 25% Rh2 lp-NDs (1×10^{12} particles/mL) were separately incubated with plasma (1:3 *v*/*v*) for 1 h at 37 °C to form lp-NDs-protein complexes. Following the incubation, lp-NDs-protein complexes were separated by spinning at 100,000×*g* for 15 min, and the resulting pellets were rinsed thrice with PBS to eliminate any unbound protein. The PC was isolated from the lp-NDs-protein complexes by exposing them to 2% SDS in PBS for 1 h at room temperature, followed by an additional ultracentrifugation step (10 min, 1000×*g*). The PC composition and abundance on the surfaces of C lp-NDs, 25% Rd lp-NDs, and 25% Rh2 lp-NDs were evaluated through the implementation of LC−MS as mentioned before. Additionally, the aforementioned ELISA methods were employed to quantify the concentrations of C3 in the PC and SC5b-9 in the plasma of C lp-NDs, 25% Rd lp-NDs, and 25% Rh2 lp-NDs, respectively.

Twelve male Sprague−Dawley (SD) rats, weighing 280 ± 20 g and aged 8 weeks, were obtained from Dossy Experimental Animals Co., Ltd. (Chengdu, China). The rats were acclimatized for one week prior to the experiment and provided ad libitum access to standard diet and water to ensure normal conditions. The animals were randomly divided into groups ($n = 3$ per group): C lp-NDs, 25% Rd lp-NDs, and 25% Rh2 lp-NDs. The lp-ND concentration was based on the injection dose of microbubble SonoVue (0.4×10^9 bubbles/kg) [Bracco, International, B.V. SonoVue, Summary of product characteristics. 2005. p. 9.]. The lp-NDs group received an intravenous injection of lp-NDs (0.4×10^9 particles/kg). The rats had unrestricted access to water but were fasted for 12 h before the experiment. Tail vein puncture was used to collect 200 μL of blood samples at 0, 5, and 60 min after administering lp-NDs, using Active Ingredient anticoagulant. The level of SC5b-9 was quantified using a rat-specific ELISA kit mentioned above.

2.13. Assay of the inhibitory effects of Gs Rd and Rh2 lp-NDs on phagocytosis

Thp-1 cells and PBMs at a concentration of 2×10^6 cells per well were plated in 6-well plates. DiI-labeled Gs and control C lp-NDs were preincubated with the same human plasma for 1 h to covered PC, then added to the cell medium at a final concentration of 1×10^9 particles/mL. After 1-h incubation in the incubator, the cells were washed thrice with sterile saline to remove any unbound lp-NDs. Subsequently, the cells were stained with fluorescent dyes for lysosomes and nuclei, fixed, and then examined by CLSM. Flow cytometry was used to evaluate cells detached using trypsin−EDTA, which were incubated with lp-NDs labeled with DiI to quantify the results.

2.14. Pharmacokinetics analysis

To establish the blood circulation patterns of Gs lp-NDs, pharmacokinetics properties of all the lp-NDs in SD rats (8 weeks, 280 ± 20 g, male) were evaluated. To this end, DiI-labeled 25% Rd, 25% Rh2, and control C lp-NDs were injected through the tail vein based on their weight (0.4×10^9 particles/kg). Blood samples were collected at specific time intervals after drug administration using a tail vein, and diluted with 1 × PBS in a 96-well plate. The diluted samples were measured using fluorescence spectrometry (549/565 nm) with three replicates for each lp-NDs fluorescence intensity on a SynergyH1 instrument (BioTek Instruments, Winooski, VT, USA). The intervals at which blood was sampled included 2, 5, 15, and 30 min, and 1, 3, 6, 12, 24, and 48 h.

A gross fluorescence imaging was used to evaluate the *in vivo* distribution of Gs lp-NDs in rats. Rats were administered 25% Rd lp-NDs, 25% Rh2 lp-NDs, and control C lp-NDs *via* the tail vein, according to their body weight (0.4×10^9 particles/kg), respectively. After induction of isoflurane anesthesia (RWD, R510-22, Shenzhen, China), the rats were subsequently humanely euthanized *via* cervical dislocation at different time points post-administration. Their lungs, hearts, kidneys, spleens, and livers were quickly removed and washed with saline. The organs were weighed and examined for particle distribution using an IVIS Spectrum *in vivo* fluorescence system (Xenogen Corp., Alameda, CA, USA), and measured the total fluorescence intensity per unit tissue mass (TFI/organ mass [g]). Subsequently, the major MPS-associated organs (liver, lung and spleen) were weighed,

Table 4 The volume of components added in anti-complement assay of the alternative pathway (μL).

Group	Gs test	Gs control	Complement	100% lysis
GVB-Mg-EGTA	−	350	150	−
Gs solution	150	150	−	−
Human serum	150	−	150	−
0.5% ERs	200	−	200	200
Ultrapure water	−	−	−	300

GVB-Mg-EGTA, veronal buffer saline containing 0.1% gelatin, 2.5 mmol/L $MgCI_2$ and 8 mmol/L EGTA); Gs, ginsenoside; RERs, rabbit erythrocytes; −, not applicable.

Please cite this article as: Zhou Jie et al., Ginsenoside modified lipid-coated perfluorocarbon nanodroplets: A novel approach to reduce complement protein adsorption and prolong *in vivo* circulation, Acta Pharmaceutica Sinica B, https://doi.org/10.1016/j.apsb.2023.11.016

homogenized at 4 °C and the total fluorescence intensity (TFI) of 25% Rd lp-NDs, 25% Rh2 lp-NDs, control C lp-NDs was assessed using a fluorescence spectrometry (549/565 nm; BioTek Instruments, SynergyMx, Winooski, VT, USA).

Furthermore, we assessed the uptake of lp-NDs by tissue-resident macrophages. Specifically, partial liver, lung and spleen were snap frozen at dissection and sent for frozen sectioning. The sliced sections were then dehydrated at 37 °C for 10−20 min. Following this, the sections were fixed with 4% paraformaldehyde in PBS at room temperature for 30 min. The sections were washed thrice on a rocking platform with PBS for 5 min per wash to remove excess fixative. Antigen retrieval was performed by immersing the sections in citrate antigen retrieval solution and subjecting them to microwave treatments: 8 min on medium power, an 8-min cooling period, and finally 7 min on low-medium power. After antigen retrieval, the sections were allowed to naturally cool. Next, three wash cycles were performed, and the tissue sections were outlined using a histological pen and blocked with BSA for 30 min. The primary antibody (anti-CD68 Rabbit pAb, diluted 1:200, Servicebio, catalog no. GB113109, Wuhan, China) was added to the sections, which were incubated overnight at 4 °C in a humid chamber. Subsequently, three wash cycles were performed, and the corresponding secondary antibody (Alexa Fluor 488-conjugated goat anti-rabbit IgG, Servicebio, catalog no. GB22301) was added and incubated at room temperature in the dark for 50 min. Slides were washed three times again. DAPI staining solution (Servicebio, catalog no. G1012) was added and incubated at room temperature for 10 min in the dark. The slides were washed three times. Finally, a fluorescence quenching agent (Servicebio, catalog no. G1401) was applied to the slides for 5 min, followed by a 10-min water rinse. Immunofluorescence sections were visualized using fluorescence microscopy (Eclipse C1, Nikon, Tokyo, Japan), and field of view was randomly selected for subsequent analysis.

2.15. In vitro *hemolysis test of Gs lp-NDs*

EDTA anticoagulated human blood was diluted with PBS, collected in hematocrit capillary tubes, and centrifuged for 5 min to determine the packed cell volume. A 2% red blood cell (RBC) suspension was prepared using the appropriate quantity of PBS. Two percent of RBC (200 μL) were incubated with C lp-NDs, 25% Rd lp-NDs, and 25% Rh2 lp-NDs at two concentrations (1×10^9 particles/mL and 1×10^{12} particles/mL) for 2 h at 37 °C. The negative control group consisted of 200 μL normal saline mixed with 200 μL of 2% RBC. The positive control group was prepared by mixing ultrapure water with 200 μL of 2% RBC to induce complete hemolysis. After incubation, the samples underwent centrifugation at 800×*g* for 3 min. After collecting 100 μL of supernatant from each sample, a reader system was used to analyze a 96-well microplate at a wavelength of 570 nm to determine the percentage of hemolysis, which was calculated using the subsequent Eq. (5):

$$\text{Percentage of hemolysis}\ (\%) = \left(\text{OD}_{\text{Sample}} - \text{OD}_{\text{Saline}}\right) / \left(\text{OD}_{\text{Complete hemolysis}} - \text{OD}_{\text{Saline}}\right) \times 100 \quad (5)$$

2.16. *Cytotoxicity assay*

The cytotoxic effects of Gs lp-NDs on differentiated Thp-1 and HUVEC cells (CellCook, catalog no. CC4004) were assayed with the cell counting kit-8 (CCK-8) kit (4A Biotech, catalog no. FXP132, Suzhou, China) according to the manufacturer's protocol. In brief, the cells were seeded onto 96-well plates and subsequently incubated at 37 °C in a 5% CO_2 environment for 24 h to facilitate attachment. Following this, the cells were exposed to C lp-NDs, 25% Rd lp-NDs, and 25% Rh2 lp-NDs for predetermined periods of 24 or 48 h, utilizing two distinct concentrations: 1×10^9 and 1×10^{12} particles/mL, respectively. Then, three rinses with PBS were performed. Subsequently, 10 μL of CCK-8 solution was added to each well and incubated for 2 h at 37 °C. Finally, the absorbance at 450 nm was measured using a microplate reader.

2.17. *Evaluation of biological safety*

SD rats (8 weeks, 280 ± 20 g) were divided into a control group administered C lp-NDs ($n = 12$), 25% Rd lp-NDs group ($n = 12$) and 25% Rh2 lp-NDs group ($n = 12$). At 0, 24, and 48 h, three rats' weights and biochemical parameters (aspartate transaminase [AST], alanine transaminase [ALT], blood urea nitrogen [BUN], creatinine [CREA] and uric acid [UA]) were evaluated. Additionally, at 0, 24, and 48 h, three rats were euthanized to procure tissue samples from the heart, liver, spleen, lung, and kidney. Organ sections (4 mm) were subjected to H&E staining for microscopic analysis.

3. Results

3.1. *Characterization of lp-NDs*

The synthetic pathway of lp-NDs is schematically presented in Fig. 1C. Lp-NDs' morphology, characterized *via* transmission electron microscope (TEM) imaging (Fig. 1D), displayed a spherical shell core structure with a discernible white mass in the center, indicating the presence of the liquid PFC core. The lp-NDs obtained exhibited a particle size of ∼400 nm and excellent stability throughout the duration of study: mean sizes of lp-NDs after synthesis and on Days 0, 1, 3, 7 and 14 were 397.94 ± 5.14 nm, 402.78 ± 4.15 nm, 398.20 ± 2.46 nm, 421.58 ± 19.96 nm and 413.51 ± 4.75 nm, respectively (each $P > 0.05$; Fig. 1E). Moreover, the PDI was approximately 0.2−0.3: PDI values after synthesis and on Days 0, 1, 3, 7 and 14 were 0.22 ± 0.02, 0.23 ± 0.02, 0.22 ± 0.02, 0.26 ± 0.03 and 0.28 ± 0.02 nm, respectively (each $P > 0.05$; Fig. 1E). The formulated lp-NDs possessed a slight negative ZP (−6.92 ± 2.72 mV), which could be attributed to inclusion of the negatively charged lipid DSPE-mPEG2000. This feature contributes to the physical stability of lp-NDs, preventing aggregation and fusion. The lp-NDs lacking DSPE-mPEG2000 exhibited a nearly neutral surface charge (−0.32 ± 1.23 mV) and significant particle aggregation under TEM (Supporting Information Fig. S3).

3.2. *Lp-NDs opsonized with C3 in plasma and activate the AP*

Exposure of lp-NDs to Active Ingredient plasma resulted in the adsorption of the PC enriched with C3 (Fig. 2A, Supporting Information Table S1), with stoichiometric analysis indicating binding of 44.17 C3 molecules per lp-ND. The KEGG enrichment analysis revealed that the term "complement and coagulation cascades" was highly enriched (Fig. 2B).

Activation of the initial part of the complement cascade was evaluated by the quantities of the C3 (Fig. 2C). Upon inhibition of

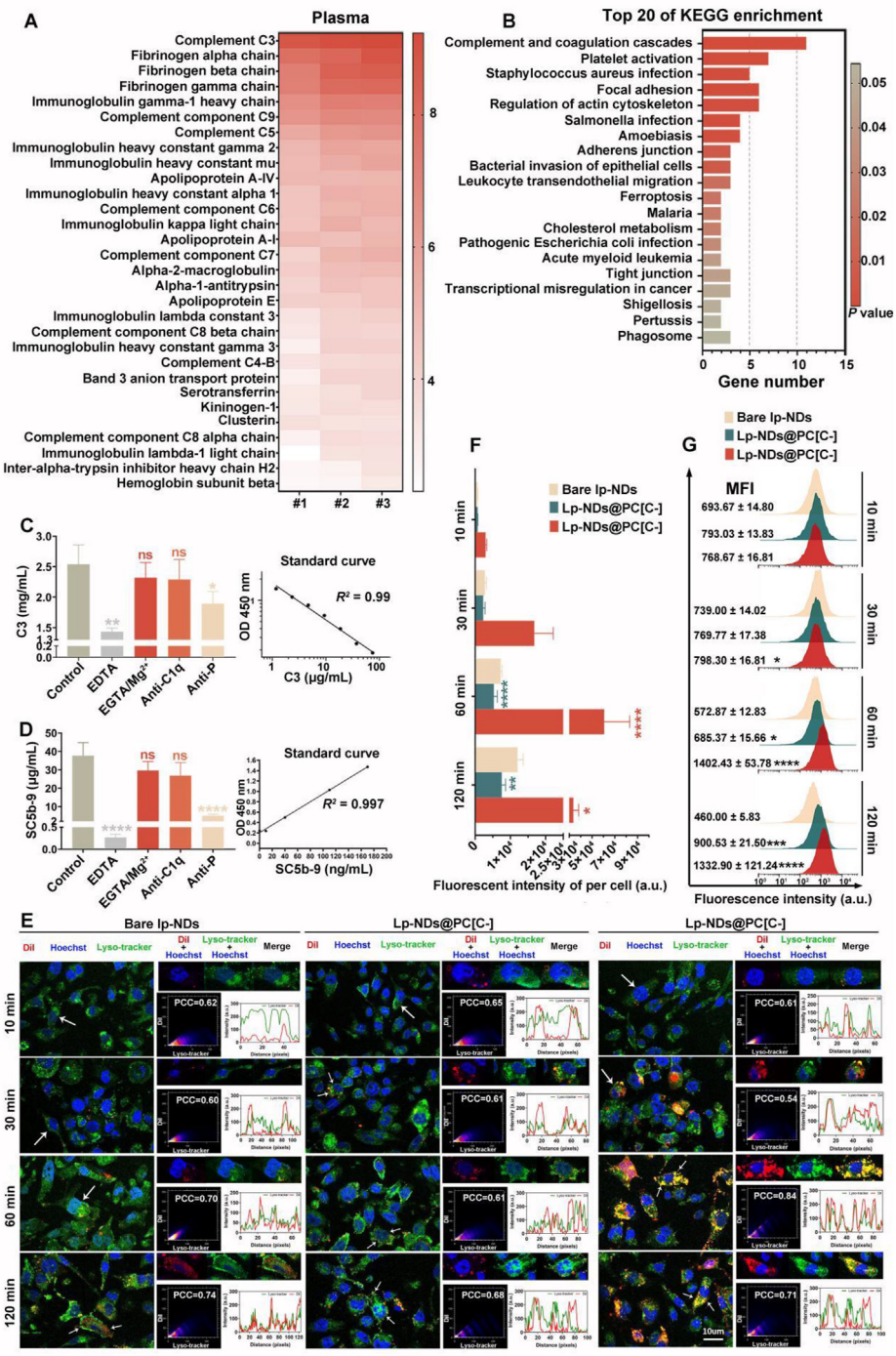

Figure 2 Influence of complement-mediated surface protein corona (PC) on phagocytosis of lp-NDs: formation and characterization. (A) Heat map of the top 30 plasma proteins identified as components of the PC formed on lp-NDs. The values in heat map indicate the logarithmically transformed label-free quantification (LFQ) detected by LC−MS, multiplied by 2. #1−3 indicate three distinct plasma samples. (B) Top 20 KEGG enrichment pathways. (C) Inhibition of complement pathway by different blockers: EDTA inhibits all pathways, EGTA/Mg^{2+} specifically inhibits Ca^{2+}-sensitive pathways, anti-C1q antibody inhibits the classical pathway (CP), anti-properdin (anti-P) antibody inhibits the alternative pathway (AP), and PBS was used as the control group. C3 levels in the PC are quantified by enzyme-linked immunosorbent assay (ELISA). The accompanying graph illustrates the standard curve for C3. (D) Following the inhibition of complement pathway by different blockers, the SC5b-9 levels in plasma incubated with lp-NDs are assessed by ELISA. The accompanying graph displays the standard curve for SC5b-9. (E) Effects of complement components on phagocytosis observed *via* confocal laser scanning microscopy. Three groups: bare lp-NDs, lp-NDs@PC [C-] (lp-NDs with protein corona lacking complement components) and lp-NDs@PC [C+] (lp-NDs with a protein corona containing complete complement components) interact with macrophages for 10, 30, 60 and 120 min, respectively. The lp-NDs are labeled with DiI (red), nucleus are labeled with Hoechst (blue) and lysosomes are labeled with Lyso-tracker (green). Single cell (arrow) higher magnification boxed areas are shown on the upper right, beneath color scatter plots corresponding to the whole images, line-scan intensity curves corresponding to the single cell

Please cite this article as: Zhou Jie et al., Ginsenoside modified lipid-coated perfluorocarbon nanodroplets: A novel approach to reduce complement protein adsorption and prolong *in vivo* circulation, Acta Pharmaceutica Sinica B, https://doi.org/10.1016/j.apsb.2023.11.016

the complement system with EDTA, only 1.43 ± 0.06 mg/mL C3 was generated, which exhibited a substantial decrease compared to the control group (C3 in the complete PC of control was 2.54 ± 0.32 mg/mL, $P < 0.01$). Neither EGTA/Mg^{2+} (2.32 ± 0.25 mg/mL, $P = 0.40$) nor anti-C1q antibody (2.29 ± 0.33 mg/mL, $P = 0.40$) inhibited C3 opsonization, while anti-P antibody (1.89 ± 0.20 mg/mL, $P < 0.05$) significantly inhibited C3 opsonization compared to the control group. Our findings indicate that C3 opsonization predominantly initiates complement activation through the AP. The deposition of human C3 on lp-NDs PC was reduced by 43.62% with EDTA and by 25.52% with anti-P antibody. The small amount of C3 observed may be attributed to plasma-intrinsic C3.

The soluble terminal complement complex (SC5b-9) was used to evaluate the terminal activation of the complement cascade (Fig. 2D). Compared to the control group (37.68 ± 7.15 μg/mL), the levels of SC5b-9 were notably reduced in both EDTA chelated plasma (0.27 ± 0.07 μg/mL, $P < 0.001$) and anti-P plasma (5.01 ± 0.90 μg/mL, $P < 0.001$). Conversely, there were no notable variations in SC5b-9 concentrations between the control plasma and EGTA/Mg^{2+} (29.65 ± 4.88 μg/mL, $P = 0.35$) or anti-C1q plasma (26.89 ± 1.06 μg/mL, $P = 0.14$) groups. SC5b-9 production was decreased by > 99% using EDTA and 86.69% using anti-P antibody. In summary, our findings provide evidence for the activation of the AP by lp-NDs.

3.3. *Complement component proteins covering lp-NDs contribute to phagocytosis*

The specific roles of the deposited complement components in phagocytosis of lp-NDs were further investigated. Specifically, DiI-labeled lp-NDs were incubated with different pretreated plasma (plasma pre-incubated with PBS or EDTA) and PBS to generate lp-NDs@PC [C+] (lp-NDs with protein corona containing complete complement components), lp-NDs@PC [C-] (lp-NDs with protein corona not containing complement component) and bare lp-NDs, respectively, and added to Thp-1 cells. To determine whether lp-NDs simply adhere to the cell surface or undergo internalization, non-phagocytic NCI−H1299 cells were also exposed to lp-NDs and compared with Thp-1 cells. After thorough washing of cultures, CLSM images revealed that nearly all lp-NDs disappeared from the medium of NCI−H1299 cells (Supporting Information Fig. S4). In contrast, lp-NDs were internalized by Thp-1 macrophages and co-localized with lysosomes (Fig. 2E).

The uptake of lp-NDs@PC [C+] was higher than that of bare lp-NDs and lp-NDs@PC [C-] at 60 and 120 min, especially at 60 min (Fig. 2E and F). However, no significant differences were observed in phagocytic uptake between bare lp-NDs and lp-NDs@PC [C-] based on mean fluorescence intensity (MFI) of per cell quantitative analysis at 10, 30, 60 and 120 min (all $P > 0.05$; Fig. 2F). Regarding the subcellular localization of lp-NDs, our initial aim was to validate their intracellular presence using lysosomal fluorescence probe. However, we made an intriguing observation that lp-NDs exhibited partial co-localization with lysosomes (Fig. 2E), as evidenced by a Pearson's correlation coefficient (PCC) exceeding 0.50. Notably, lp-NDs@PC [C+] demonstrated the highest PCC (0.84) after 60 min, coinciding with the highest phagocytotic MFI. Furthermore, in the fluorescence co-localization position−intensity diagram, lp-NDs@PC [C+] after 60 min also exhibited more overlapping curves.

To compare internalization of lp-NDs by Thp-1 cells, flow cytometry analysis was conducted. As depicted in Fig. 2G, the histogram and MFI quantitative analysis demonstrated increased uptake of lp-NDs@PC [C+] at 60 and 120 min compared to bare lp-NDs and lp-NDs@PC [C-] (all $P < 0.05$), clearly suggesting that complement production plays a role in enhancing phagocytosis.

3.4. *Anti-complement effect of Gs* in vitro

Anti-complement hemolysis assay of CP revealed that Gs Rd and Rh2 were ineffective in inhibiting hemolysis, with inhibition rates not exceeding 10% (shown in Fig. 3A and B). For the AP, hemolysis inhibition rates were 41.01 ± 1.59%, 23.21 ± 0.57%, 13.53 ± 0.54%, 9.97 ± 1.56%, 6.86 ± 0.27%, 5.76 ± 0.38%, 4.87 ± 0.63% and 0.19 ± 1.66% at Gs Rd dilution ratios of 1:1, 1:2, 1:4, 1:8, 1:16, 1:32, 1:64 and 1:128, respectively (Fig. 3C), suggesting inhibition of the AP to some extent. Hemolysis inhibition rates by Gs Rh2 were 52.77 ± 0.57%, 35.27 ± 0.56%, 28.47 ± 0.63%, 23.74 ± 0.10%, 18.48 ± 0.63%, 10.66 ± 0.55%, 1.34 ± 2.01%, and 0% at dilution ratios of 1:1, 1:2, 1:4, 1:8, 1:16, 1:32, 1:64 and 1:128, respectively (Fig. 3D), similarly indicating that Rh2 exerts an inhibitory effect on the AP. Our findings suggest that Rd and Rh2 monomers are capable of inhibiting the AP of complement *in vitro*.

3.5. *Preparation of Gs lp-NDs*

Schematic diagram of Gs lp-NDs is illustrated in Fig. 4A. In brief, Gs lp-NDs comprise a core consisting of C_6F_{14} enveloped by a lipid shell modified with Gs. TEM images revealed a typical spherical shell/core morphology (Fig. 4B). Particles of 75% Rd lp-NDs and 75% Rh2 lp-NDs imaged *via* TEM were deformed, shriveled and ruptured, which could be attributed to the effects of the thermal electron beam utilized during imaging. Particle size, PDI, and ZP of Gs lp-NDs were assessed promptly subsequent to their synthesis (Fig. 4C−E, Table 5). The sizes of all Gs lp-NDs ranged from 384.65 ± 18.59 nm to 408.80 ± 5.21 nm, and no significant statistical differences (all $P > 0.05$; Fig. 4C) were found. PDI ranged from 0.19 ± 0.05 to 0.27 ± 0.05, with no significant statistical differences (all $P > 0.05$; Fig. 4D). Our results indicate that particle size is well regulated with a narrow dispersity (PDI value < 0.3). Nonetheless, our findings indicate that Gs lp-NDs with higher concentrations of Gs display larger negative ZP (Fig. 4E), which could be explained by the negative groups present in the Gs structure.

Regarding the stability of the formulation, regardless of Rd and Rh2, notable fluctuations in the diameter of particles for both 50% and 75% Gs lp-NDs were detected during the 14-day storage duration at 4 °C (Fig. 4F). However, no significant variations were

images (arrow). The intracellular co-localization between lp-NDs and lysosomes is assessed using the Pearson correlation coefficient (PCC). Scale bar = 10 μm. (F) Quantification of Thp-1 cells' uptake based on fluorescence intensity of per cell (a.u.) obtained from confocal laser scanning microscopy images of bare lp-NDs, lp-NDs@PC [C-] and lp-NDs@PC [C+] at 10, 30, 60, and 120 min. (G) Flow cytometry mean fluorescence intensity (MFI) of cellular uptake of bare lp-NDs, lp-NDs@PC [C-] and lp-NDs@PC [C+] at 10, 30, 60, and 120 min. Data are presented as mean ± SD ($n = 3$), ns, not significant. *$P < 0.05$, **$P < 0.01$, ***$P < 0.001$. ****$P < 0.0001$.

Please cite this article as: Zhou Jie et al., Ginsenoside modified lipid-coated perfluorocarbon nanodroplets: A novel approach to reduce complement protein adsorption and prolong *in vivo* circulation, Acta Pharmaceutica Sinica B, https://doi.org/10.1016/j.apsb.2023.11.016

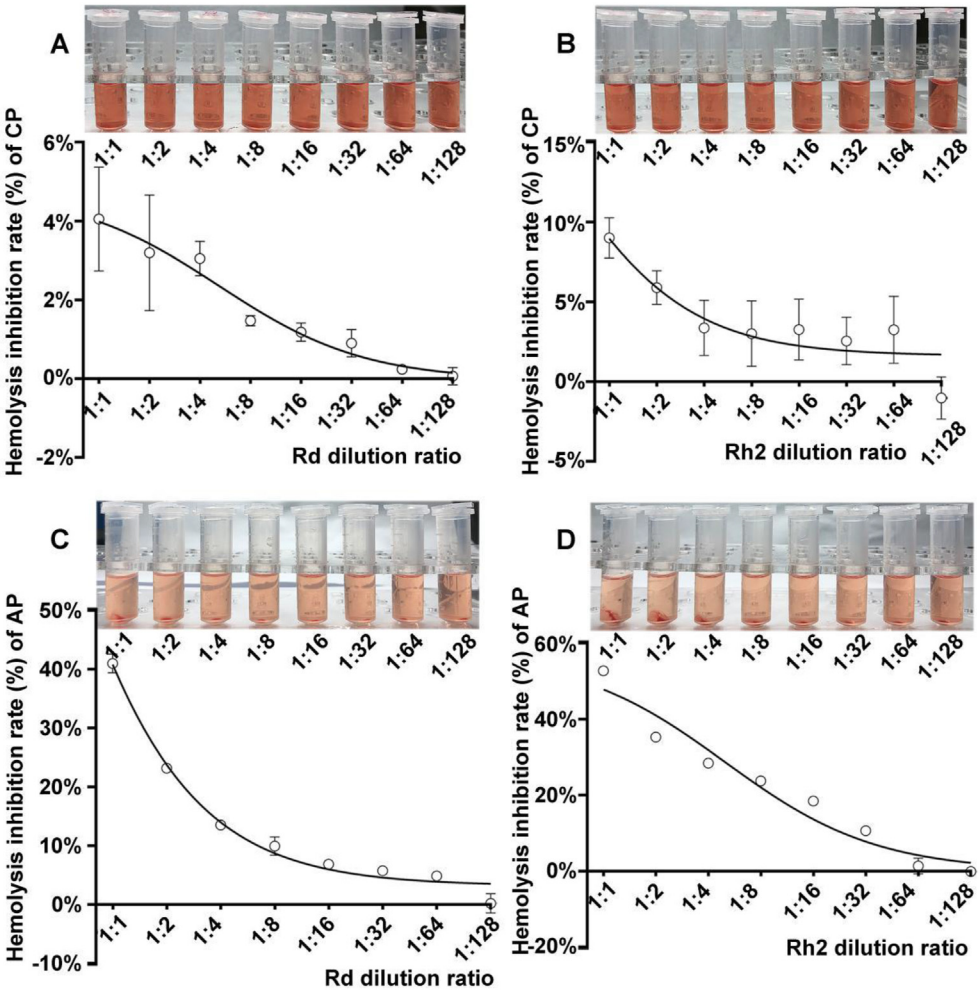

Figure 3 Assay of the anti-complement activities of ginsenoside Rd and Rh2 monomers *in vitro*. (A) Hemolysis inhibition rate of Rd in the classical pathway (CP). (B) Inhibition rate of hemolysis induced by Rh2 in the CP. (C) Hemolysis inhibition rate of Rd in the alternative pathway (AP). (D) Inhibition rate of hemolysis induced by Rh2 in the AP. Data are presented as mean ± SD (n = 3).

observed in size (Fig. 4F), PDI (Fig. 4G), and ZP (Fig. 4H) of 25% Gs lp-NDs, indicating superior stability of this formulation.

3.6. *Encapsulation test*

Ginsenoside Rd and Rh2 contain a C=C structure and exhibit different infrared spectra to DPPC and DPPS-mPEG2000. FTIR spectroscopy was further conducted to verify encapsulation of Gs in Gs lp-NDs. The molecular structure of the shell materials is depicted in Fig. 5A. As shown in Fig. 5B and C, several peaks were prevalent in the spectra of Gs lp-NDs. Peaks at 1644 cm^{-1} could be ascribed to the stretching vibration of the C=C structure observed in Gs and all Gs lp-ND samples. These peaks were absent in C lp-NDs, indicating the successful loading of Gs on lp-NDs. In addition, characteristic peaks of the C=O group appeared at 1738 cm^{-1} in the spectra of C lp-NDs and all Gs lp-NDs, indicating the presence of phospholipid.

Multistage mass spectra of Gs Rd, Rh2, and Re (internal standard) are shown in Fig. 5D−F, respectively. Rd had a retention time of 3.03 min and generated an excimer ion peak at *m/z* 945.8 $[M\text{-}H]^-$, accompanied by the production of fragments at *m/z* 783.2 and 621.5 (Fig. 5D). In the cationic mode, the retention time of Rh2 was 3.92 min, with an excimer ion peak observed at *m/z* 623.5 $[M+H]^+$ (as shown in Fig. 5E), accompanied by the formation of fragment ions at *m/z* 587.3 and 407.5. The first-order mass spectrometry in anion mode exhibited an excimer ion peak $[M\text{-}H]^-$ with *m/z* 945.8 for Gs Re, similar to Gs Rd. However, the obtained fragment ions at *m/z* 475.4 and 637.4 were distinct, as depicted in Fig. 5F. Gs of the different formulations were subsequently quantified using the standard curve of Rd and Rh2 to determine their actual amounts in Gs lp-NDs. The chromatograms obtained for all Gs lp-NDs are depicted in Supporting Information Fig. S5. EE of 25%, 50%, and 75% Rd lp-NDs were determined as 97.23 ± 3.56%, 93.42 ± 5.16% and 92.84 ± 1.22%, respectively. EE of 25%, 50%, and 75% Rh2 lp-NDs were 98.04 ± 2.18%, 96.15 ± 3.03% and 99.28 ± 1.41%, respectively (Table 5).

3.7. *Anti-complement effects of Gs lp-NDs* in vitro *and* in vivo

To assess the impact of Gs lp-NDs on complement activation in PC, we conducted LC−MS analysis to examine the surface proteome composition of C lp-NDs, 25% Rd lp-NDs, and 25% Rh2 lp-NDs (Fig. 6A). Our findings revealed that C3 maintained its prominence as the second most abundant protein in the C lp-NDs group. Its label-

Please cite this article as: Zhou Jie et al., Ginsenoside modified lipid-coated perfluorocarbon nanodroplets: A novel approach to reduce complement protein adsorption and prolong *in vivo* circulation, Acta Pharmaceutica Sinica B, https://doi.org/10.1016/j.apsb.2023.11.016

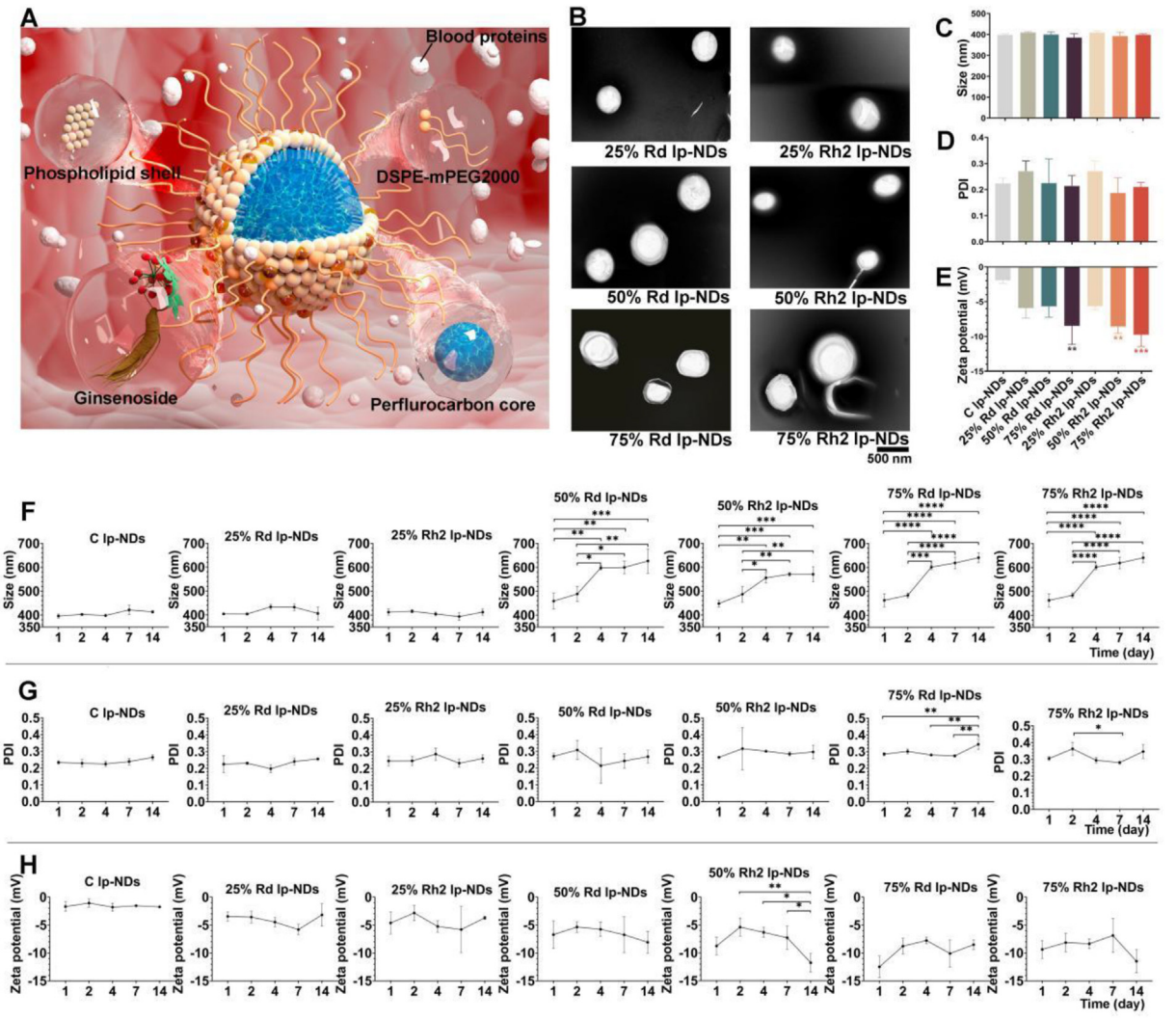

Figure 4 Characterization of Gs lp-NDs. (A) Schematic diagram of Gs lp-NDs. (B) Transmission electron microscopy images of different Gs lp-ND formulations. Scale bar = 500 nm. (C) Particle size of different Gs lp-ND formulations after preparation. (D) Polydispersity index (PDI) of different Gs lp-ND formulations following their preparation. (E) Zeta potential (ZP) of different Gs lp-ND formulations after preparation. (F) Mean particle size of different Gs lp-NDs on Days 1, 2, 4, 7, and 14. (G) PDI of different Gs lp-NDs on Days 1, 2, 4, 7, and 14. (H) ZP of different Gs lp-ND formulations on Days 1, 2, 4, 7, and 14. Data are presented as mean ± SD ($n = 3$). *$P < 0.05$, **$P < 0.01$, ***$P < 0.001$. ****$P < 0.0001$.

free quantification (LFQ) intensity was determined to be $5.06 \times 10^9 \pm 1.70 \times 10^8$, indicating a substantial presence. Although C3 was not the most abundant protein, its abundance was only slightly lower than that of the most abundant protein, immunoglobulin kappa constant ($5.08 \times 10^9 \pm 3.85 \times 10^8$), and this difference did not reach statistical significance ($P = 0.3247$). In contrast, the analysis of 25% Rd lp-NDs and 25% Rh2 lp-NDs groups revealed a notable shift in the abundance of C3 protein. It no longer remained among the top five most abundant proteins, instead ranking as the sixth and eighth most abundant proteins in these groups. The quantitative LFQ intensity of C3 in the three groups demonstrated a notable decrease in C3 abundance in both the 25% Rd lp-NDs and 25% Rh2 lp-NDs groups ($2.68 \times 10^9 \pm 7.00 \times 10^8$, $2.07 \times 10^9 \pm 4.81 \times 10^7$, respectively) compared to the control group (Fig. 6B). These differences were found to be statistically different, with P values less than 0.01 and 0.001, respectively.

Additionally, the levels of C3 and SC5b-9 were quantified *in vitro*. The concentrations of C3 in the PC of 25% Rd lp-NDs and 25% Rh2 lp-NDs PC were 2.41 ± 0.24 mg/mL and 2.26 ± 0.54 mg/mL, respectively (Fig. 6C), which are statistically lower than that in the C lp-NDs (3.58 ± 0.41 mg/mL; $P < 0.05$). Plasma SC5b-9 levels were additionally measured to assess terminal complement activation (Fig. 6D). Plasma concentrations of SC5b-9 were statistically higher in C lp-NDs (35.85 ± 2.23 μg/mL) compared with 25% Rd lp-NDs (21.48 ± 2.58 μg/mL, $P = 0.0008$) and 25% Rh2 lp-NDs (15.89 ± 2.30 μg/mL, $P = 0.0001$).

In vivo measurement of SC5b-9 generation after Gs lp-NDs and C lp-NDs administration was conducted. At 5-min post-intravenous injection of lp-NDs, SC5b-9 levels remained stable across all groups. However, after 1 h, a significant increase in SC5b-9 was evident in the C lp-ND group (Fig. 6E). Notably, the

Please cite this article as: Zhou Jie et al., Ginsenoside modified lipid-coated perfluorocarbon nanodroplets: A novel approach to reduce complement protein adsorption and prolong *in vivo* circulation, Acta Pharmaceutica Sinica B, https://doi.org/10.1016/j.apsb.2023.11.016

Table 5 Characterization of different lp-NDs.

Add heading	Size (nm)	PDI	ZP (mV)	EE (%)
Lp-NDs/C lp-NDs	397.94 ± 5.15	0.22 ± 0.02	−6.92 ± 2.72	–
75% Rd lp-NDs	384.65 ± 18.59	0.21 ± 0.04	−8.47 ± 2.69	92.84 ± 1.22
50% Rd lp-NDs	399.45 ± 12.29	0.22 ± 0.09	−5.68 ± 1.57	93.42 ± 5.16
25% Rd lp-NDs	408.80 ± 5.21	0.27 ± 0.05	−5.92 ± 1.44	97.23 ± 3.56
75% Rh2 lp-NDs	398.34 ± 4.99	0.21 ± 0.02	−9.47 ± 1.71	99.28 ± 1.41
50% Rh2 lp-NDs	391.54 ± 19.10	0.19 ± 0.05	−8.57 ± 0.99	96.15 ± 3.03
25% Rh2 lp-NDs	408.68 ± 7.17	0.27 ± 0.04	−5.64 ± 0.53	98.04 ± 2.18

SD, standard deviation; PDI, polydispersity index; ZP, zeta potential; EE encapsulation efficiency; –, not applicable. Data are presented as mean ± SD (n = 3).

C lp-ND group exhibited the highest level of SC5b-9 (0.161 ± 0.015 mAU/mL) exceeding those of 25% Rd lp-NDs (0.129 ± 0.007 mAU/mL, P = 0.46) and 25% Rh2 lp-NDs (0.084 ± 0.011 mAU/mL, P = 0.0017), although the difference between C lp-ND and 25% Rd lp-ND groups was not significant.

3.8. *Anti-phagocytosis effects of Gs lp-NDs* in vitro *and* in vivo

3.8.1. *Cellular uptake* in vitro

The cellular uptake of C lp-NDs and Gs lp-NDs by Thp-1 cells and PBMs is illustrated in Fig. 6F and I, respectively. In the C lp-NDs group, particles manifested increased fluorescence (red) within both cells, exhibiting a distinct localization within lysosomes (green). Data from MFI analysis showed that Thp-1 cells internalized a higher number of C lp-NDs than Gs lp-NDs (Fig. 6G, both $P < 0.01$). The MFI value of C lp-NDs in Thp-1 cells was found to be 3.29-fold higher than that of 25% Rd lp-NDs and 14.34-fold higher than that of 25% Rh2 lp-NDs (Fig. 6G). Similarly, in PBMs, the MFI value of C lp-NDs was 4.19-fold higher than that of 25% Rd lp-NDs and 9.56-fold higher than that of 25% Rh2 lp-NDs (Fig. 6J, both $P < 0.001$).

Complementary results were obtained from flow cytometry experiments, as depicted in Fig. 6H and K. In Thp-1 cells, the MFI of the C lp-ND group (6360.37 ± 233.74) was significantly higher compared to 25% Rd lp-NDs (4775.13 ± 190.83, $P < 0.0001$) and 25% Rh2 lp-NDs (5007.03 ± 122.27, $P < 0.0001$), indicating a reduced phagocytic uptake of particles after Gs added. Similarly, in PBMs, the MFI of the C lp-ND group (7133.63 ± 433.86) was also significantly higher than that of 25% Rd lp-NDs (3625.23 ± 132.66, $P < 0.0001$) and 25% Rh2 lp-NDs (3331.73 ± 151.81, $P < 0.0001$).

For the co-localization of lp-NDs and lysosome, in both Thp-1 cells (Fig. 6F) and PBMs (Fig. 6I), the three types of lp-NDs showed a different degree of overlap with lysosomes, as observed by the yellow fluorescence resulting from the merging of lysosomes (green) and lp-NDs (red). Additionally, both PCC values and plot profile analysis revealed that all three lp-NDs exhibited partial localization properties within lysosomes in both Thp-1 cells and PBMs, with PCC values of about 0.6 and 0.5, respectively.

3.8.2. *Gs lp-NDs exhibit prolonged blood circulation and reduced accumulation in lung and liver*

The fluorescence intensities of lp-NDs in blood samples taken at various times after intravenous injection (2, 5, 10 and 30 min, and 1 h, as well as 3, 6, 12, 24 and 48 h) were used to determine the concentrations of Gs lp-NDs and C lp-NDs in circulation. Following injection, 25% Rd lp-NDs and 25% Rh2 lp-NDs displayed extended blood retention at 2, 5, 10, 30 min, and 1 h compared to C lp-NDs (Fig. 7A). The circulation half-lives of 25% Rd lp-NDs and 25% Rh2 lp-NDs were determined as 186.40 and 54.68 min, respectively, which were longer than that of C lp-NDs (21.73 min).

The distribution was evaluated using an *in vivo* fluorescence system. Following injection, fluorescence density was detected in

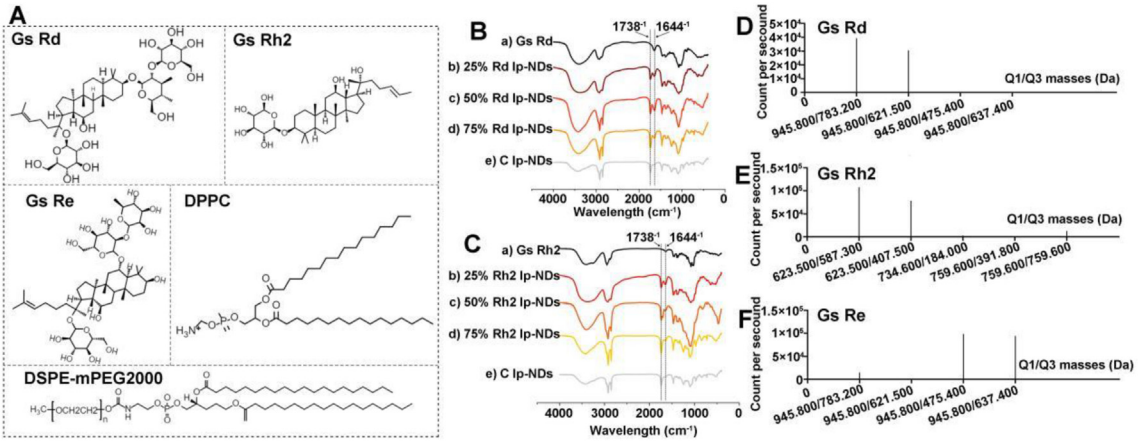

Figure 5 Encapsulation test of Gs lp-NDs. (A) Chemical structures of ginsenoside Rd (Gs Rd), ginsenoside Rh2 (Gs Rh2), ginsenoside Re (Gs Re), DPPC and DSPE-mPEG2000. (B) Fourier-transform infrared (FT-IR) spectroscopy of Gs Rd lp-NDs. (C) FT-IR spectroscopy of Gs Rh2 lp-NDs. (D) Multistage mass spectra of Gs Rd. (E) Multistage mass spectra of Gs Rh2. (F) Multistage mass spectra of Gs Re.

Please cite this article as: Zhou Jie et al., Ginsenoside modified lipid-coated perfluorocarbon nanodroplets: A novel approach to reduce complement protein adsorption and prolong *in vivo* circulation, Acta Pharmaceutica Sinica B, https://doi.org/10.1016/j.apsb.2023.11.016

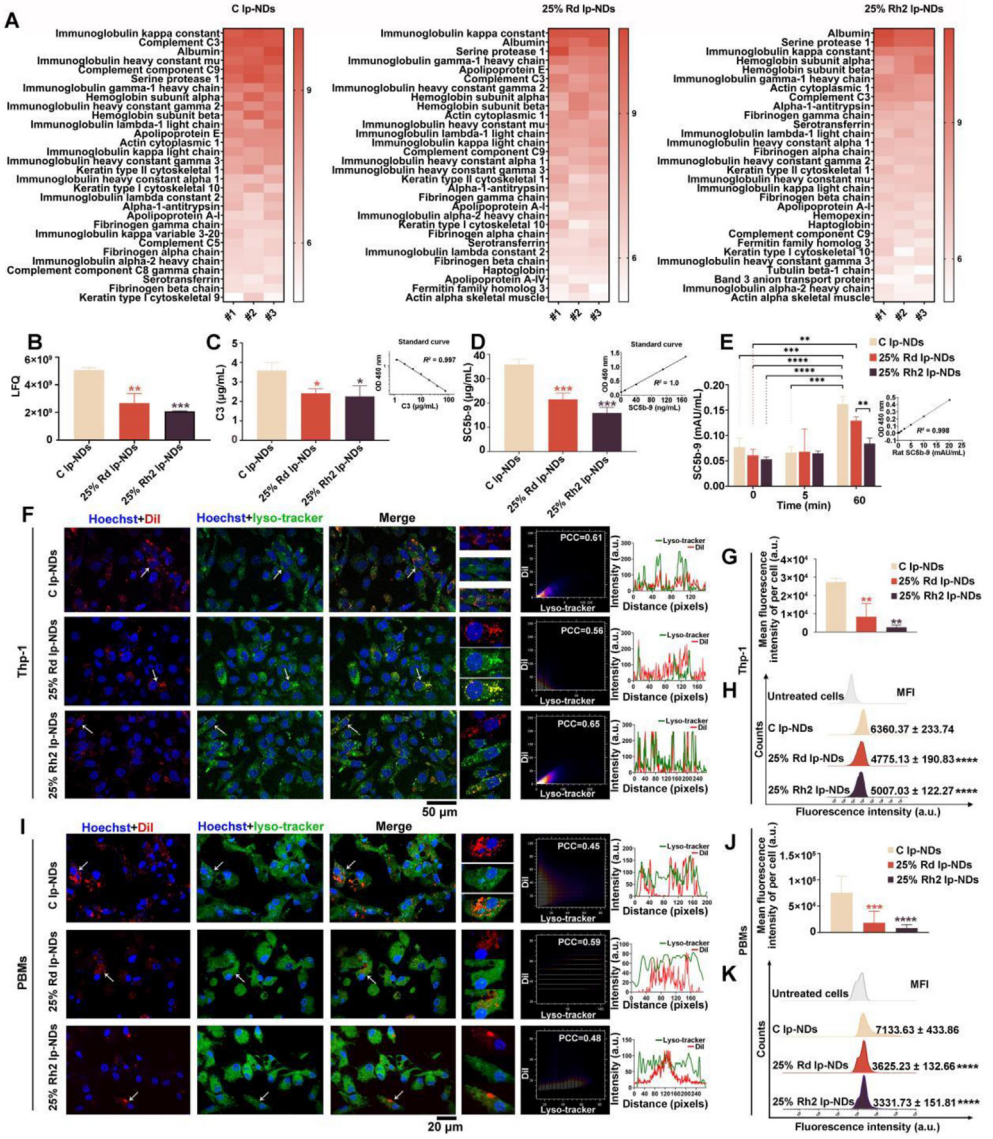

Figure 6 Anti-complement and anti-macrophage effect of Gs lp-NDs. (A) Top 30 plasma proteins identified by PC LC−MS analysis of C lp-NDs, 25% Rd lp-NDs, and 25% Rh2 lp-NDs. The values in heat map indicates the logarithmically transformed label-free quantification (LFQ) multiplied by 2. #1−3 indicates three different plasma samples. (B) The LFQ of C3 in C lp-NDs, 25% Rd lp-NDs, and 25% Rh2 lp-NDs. (C) *In vitro* human C3 in PC of C lp-NDs, 25% Rd lp-NDs and 25% Rh2 lp-NDs. (D) *In vitro* human SC5b-9 generation following plasma incubation with C lp-NDs, 25% Rd lp-NDs, and 25% Rh2 lp-NDs. (E) *In vivo* SC5b-9 production in rats following injection with C lp-NDs, 25% Rd lp-NDs, and 25% Rh2 lp-NDs. (F) Uptake of C lp-NDs and Gs lp-NDs by Thp-1 cells. Lysosomes of THP-1 cells, cell nuclei, and lp-NDs are labeled with green, blue, and red fluorescent dye, respectively. Scale bar = 50 μm. (G) Quantification of Thp-1 cell uptake based on mean fluorescence intensity (MFI) values of each cell obtained from confocal laser scanning microscopy (CLSM) images. (H) Cell counts/fluorescence intensity histogram and relevant MFI of Thp-1 cells uptake C lp-NDs and Gs lp-NDs, determined *via* flow cytometry. (I) Internalization of C lp-NDs and Gs lp-NDs by peripheral blood macrophages (PBMs). Lysosomes within PBMs cells, cell nuclei, and lp-NDs are fluorescently labeled with green, blue, and red dyes, respectively. Scale bar = 20 μm. (J) Quantification of PBMs cell uptake by determining the MFI values for each cell, based on analysis of CLSM images. (K) Flow cytometer analysis of the histogram depicting PBMs cell count and fluorescence intensity, along with the corresponding MFI, illustrating the uptake of C lp-NDs and Gs lp-NDs by PBMs. Data are presented as mean ± SD ($n = 3$). *$P < 0.05$, **$P < 0.01$, ***$P < 0.001$. ****$P < 0.0001$.

the lung, liver, spleen, kidney and heart. As shown in Fig. 7B, both Gs lp-NDs and C lp-NDs were primarily distributed in lung, liver, spleen, and kidney, but not heart. As shown in Fig. 7C, in the lung, TFI/weight (/g) of C lp-NDs reached peak levels 10 min after injection, which was an earlier time-point compared to all Gs lp-ND groups (peak time 1 and 3 h for 25% Rd lp-NDs and 25% Rh2 lp-NDs, respectively). The highest TFI/weight of C lp-NDs was 4.06 times greater than that of 25% Rd lp-NDs and 2.01 times greater than that of 25% Rh2 lp-NDs in the lung. In liver, TFI/weight of both C lp-ND and 25% Rh2 lp-ND groups attained maximal levels at 6 h. In contrast, the peak time of 25% Rd lp-NDs was earlier, and highest TFI/weight was lower than that of C lp-NDs and 25% Rh2 lp-NDs. Interestingly, in the spleen, TFI/weight of both 25% Rd lp-ND and 25% Rh2 lp-ND groups were

Please cite this article as: Zhou Jie et al., Ginsenoside modified lipid-coated perfluorocarbon nanodroplets: A novel approach to reduce complement protein adsorption and prolong *in vivo* circulation, Acta Pharmaceutica Sinica B, https://doi.org/10.1016/j.apsb.2023.11.016

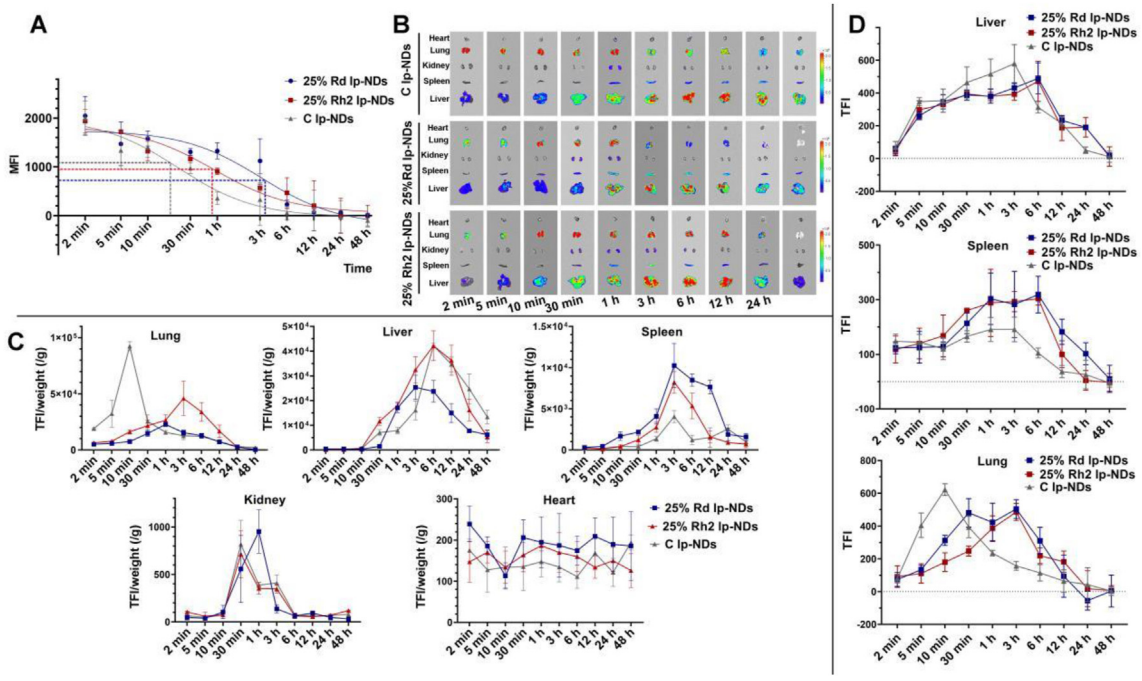

Figure 7 Metabolism of Gs lp-NDs. (A) Mean fluorescence intensity (MFI) of Gs lp-NDs and C lp-NDs in the blood circulation. (B) Distribution of Gs lp-NDs and C lp-NDs in internal organs of rats. (C) Total fluorescence intensity/weight (TFI/weight) of C and Gs lp-NDs in rat lung, liver, spleen, kidney and heart. (D) The TFI of fluorescent-labeled lp-NDs in the homogenized samples derived from liver, spleen and lung. Data are presented as mean ± SD ($n = 3$).

3.69 and 1.8 times higher, respectively, than the C lp-ND group, with a similar peak time of 3 h. Furthermore, the kidney accumulation of lp-NDs was significantly lower compared to that in the lung, liver, and spleen. Additionally, a notable minimal accumulation of lp-NDs was observed in the heart.

Given the significance of the liver, spleen, and lungs as pivotal organs within the MPS, housing a multitude of tissue-resident phagocytes, we conducted an in-depth analysis to examine the abundance of lp-NDs in the homogenized samples derived from these tissues. As depicted in Fig. 7D, a discernible pattern of gradual hepatic accumulation was evident across all three lp-NDs, demonstrating a sustained increase within the liver following administration. The culmination of this accumulation was observed at about 3 and 6 h, respectively, with the peak of the C lp-NDs (579.67 ± 116.32) occurring around 3 h, while the peak of the 25% Rd lp-NDs (489.33 ± 97.73) and 25% Rd lp-NDs (471.67 ± 122.65) were observed approximately 6 h post-administration. Notably, this trend was also evident in the spleen, wherein the highest TFI of C lp-NDs (191.00 ± 45.13) was evident at 3 h, while the peak TFIs of the 25% Rd lp-NDs (318.67 ± 67.00) and 25% Rd lp-NDs (303.67 ± 23.25) were observed at approximately 6 h. Moreover, the TFIs of C lp-NDs in lung homogenate reached their peak at 10 min, which was consistent with the overall fluorescence results obtained from the gross specimen (Fig. 8B and C). Furthermore, our investigation unveiled a consistent trend wherein the TFI of C lp-NDs in both the hepatic and splenic tissues exhibited a sustained elevation compared to that of 25% Rd lp-NDs and 25% Rh2 lp-NDs, although this disparity did not reach statistical significance (all $P > 0.05$). We hypothesize that the lack of statistical difference could potentially be attributed to inherent limitations in tissue homogenization experiments, which may inadvertently affect the integrity of lp-NDs during the homogenization process. To minimize potential damage to lp-NDs during tissue homogenization, we implemented immunofluorescence detection by labeling macrophages in tissue slices. This approach provided a slightly more precise evaluation of lp-ND engulfment within the tissues. However, it is important to emphasize certain limitations associated with the assessment of immunofluorescence detection using sections. The primary limitation arose from the inhomogeneous distribution of lp-NDs in organs. To address this, we implemented a random selection process involving CD68-negative tissue cells and CD68-positive macrophages for fluorescence image and semi-quantitative analysis. The results exhibited a notable likeness to the TFI observed in tissue homogenate, despite some standard deviations displaying a substantial range, resulting in minimal statistical significance (Supporting Information Fig. S6).

3.9. *Safety of Gs lp-NDs*

The potential cytotoxicity of Gs lp-NDs was assessed using CCK-8 and hemolysis assays. The hemolysis percentage of human RBC was significantly lower than the limiting value of 5%[28], as shown in Fig. 8A, indicating excellent hemocompatibility of Gs lp-NDs. Additionally, as shown in Fig. 8B (Thp-1) and 8C (HUVEC), cell viabilities were >90% after treatment with Gs lp-NDs at both low (1×10^9 particles/mL) and high (1×10^{12} particles/mL) concentrations. These findings clearly indicate that Gs lp-NDs do not exert significant cytotoxicity *in vitro*.

To investigate the potential *in vivo* toxicity of Gs lp-NDs, we evaluated various parameters in a rat model, including changes in body weight, blood biochemical parameters, and organ histopathology. Body weight was monitored for one week following injection. The results showed a gradual increase in body weight in all groups, signifying that Gs lp-NDs do not induce body weight loss

Please cite this article as: Zhou Jie et al., Ginsenoside modified lipid-coated perfluorocarbon nanodroplets: A novel approach to reduce complement protein adsorption and prolong *in vivo* circulation, Acta Pharmaceutica Sinica B, https://doi.org/10.1016/j.apsb.2023.11.016

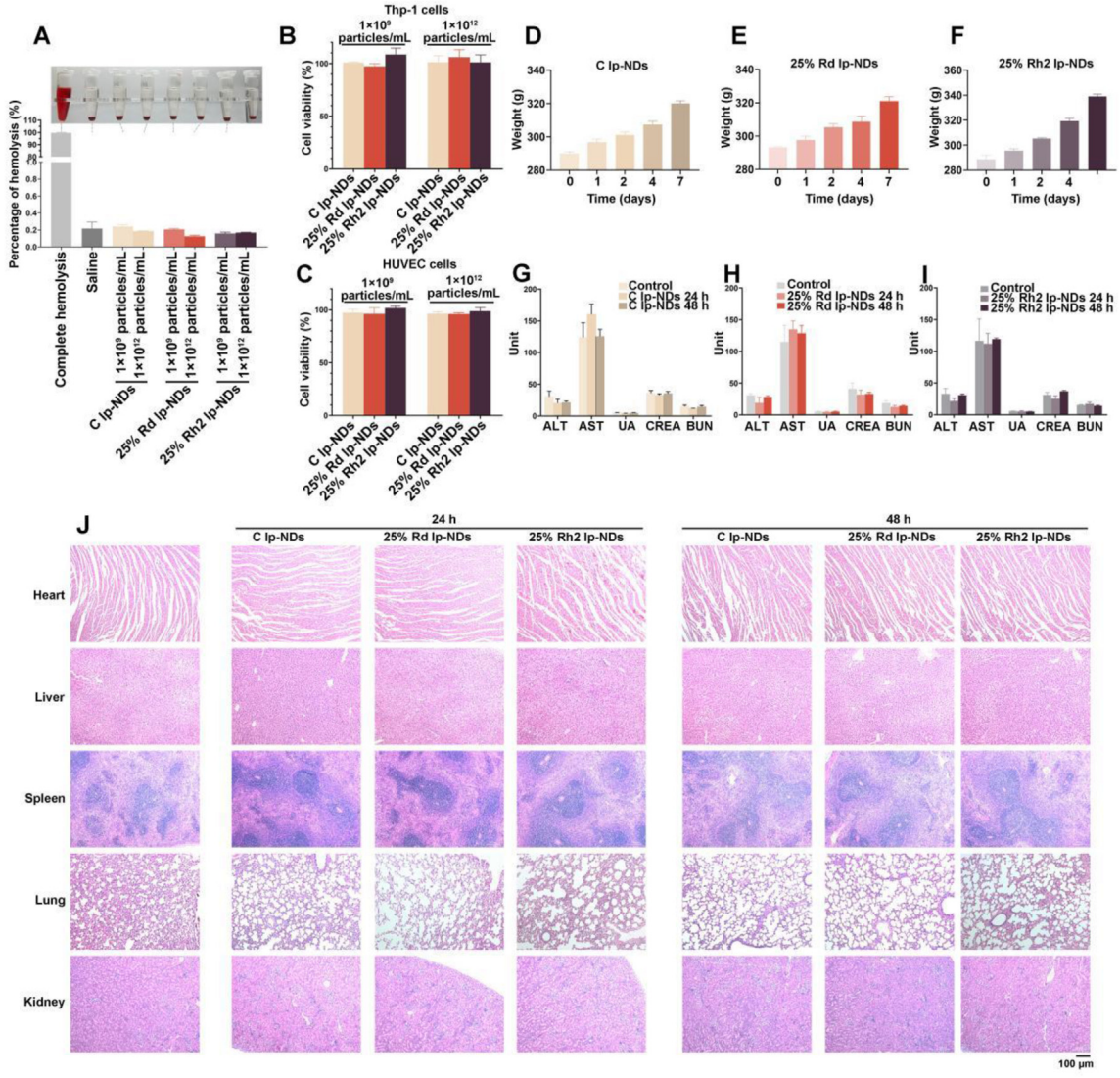

Figure 8 Biocompatibility of Gs lp-NDs. (A) Hemocompatibility of Gs lp-NDs. (B) CCK-8 assay for THP-1 and (C) HUVEC cells. (D) Body weights of rats treated with C lp-NDs, (E) 25% Rd lp-NDs and (F) 25% Rh2 lp-NDs. (G) Blood biochemical parameters of rats treated with C lp-NDs, (H) 25% Rd lp-NDs and (I) 25% Rh2 lp-NDs. (J) Histological staining of major organs at 24 and 48 h after intravenous administration of C lp-NDs and Gs lp-NDs. Scale bar = 100 μm. Data are presented as mean ± SD (n = 3).

in rats (Fig. 8D–F). Blood biochemical tests revealed no significant differences in ALT, AST, BUN, UA, and CREA levels between the experimental and control (treated with saline) groups, indicative of low toxicity of Gs lp-NDs (Fig. 8G–I). Histological staining of vital organs post intravenous administration of Gs lp-NDs after 24 and 48 h showed no significant abnormalities in the heart, liver, spleen, lung or kidney, confirming the *in vivo* low toxicity of Gs lp-NDs (Fig. 8J).

4. Discussion

Lp-NDs, also known as perfluorocarbon nanoparticles/nanoemulsions or phase-shift nanoparticles/nanoemulsions, offer a novel approach to diagnosis, therapy, and vaccine agents[4]. These nanodroplets consist of a liquid perfluorocarbon core stabilized by an emulsifier shell primarily composed of phospholipids, and can effectively serve as vehicles for targeted drug delivery with high monitoring performance, improved drug solubility and bioavailability, and controlled release kinetics in response to various external stimuli, including ultrasound, photoacoustic, microwave, and magnetic resonance imaging[1].

However, non-specific clearance by the IIS severely impedes the clinical application of lp-NDs. Willmann et al.[29] previously demonstrated that macrophages could rapidly remove lipid shell-targeted microbubbles from the bloodstream, resulting in a half-life of only 3.5 min. While limited research has focused on the pharmacokinetics of nanoscale lp-NDs, low delivery efficiency (<1%) of liposomes possessing shells similar to lp-NDs has been documented[7]. DPPC, which serves as the major component of mammalian cell membranes with excellent biocompatibility[30], was utilized as the primary membrane material in our study. However, the half-life of lp-NDs composed of DPPC was only 21.73 min (Fig. 7A), which was significantly lower than the clinical requisite half-life period of several hours[31].

Please cite this article as: Zhou Jie et al., Ginsenoside modified lipid-coated perfluorocarbon nanodroplets: A novel approach to reduce complement protein adsorption and prolong *in vivo* circulation, Acta Pharmaceutica Sinica B, https://doi.org/10.1016/j.apsb.2023.11.016

Compared to other nanomaterial types, lp-NDs require greater diameters, particularly with respect to ultrasonic imaging quality and necessary stimuli, to promote vaporization. The ideal diameter post-phase change of lp-NDs ranges from 2.5 to 4 μm[32,33]. According to the ideal gas laws, which account for surface tension effects, the expansion of a resulting bubble following vaporization of a PFC droplet is anticipated to be ∼3−6 times in diameter[34]. Accordingly, we infer that a diameter of ∼400 nm is optimal for lp-NDs, which is sufficiently small to penetrate the loose capillary space within tumor tissue. Particle size and distribution are widely recognized as important factors in drug delivery and medical imaging[35]. Particles ranging from 200 to 500 nm in diameter are more readily internalized by both phagocytic and non-phagocytic cells compared to smaller particles[7,35]. Therefore, efficacious surface modifications of lp-NDs are necessary to mitigate non-specific clearance.

The formation of the PC presents the initial biological response to nanomaterial exposure within the body and is a key factor in labeling of nanomaterials by biological systems. However, there is a lack of literature on the PC composition related to lp-NDs. Earlier research on liposome PC has provided valuable insights for design of lp-NDs. Corbo et al.[36] synthesized liposomes using a combination of DPPC, dioleoylphosphatidylcholine (DOPC) and cholesterol, and identified the top five proteins that adsorbed onto the liposome surface after murine plasma exposure: serum albumin, apolipoprotein-E, Ig mu chain C region, apolipoprotein A-IV, and myosin. Giulimondi et al.[37] demonstrated that liposomes comprised of DOTAP (1,2-dioleoyl-3-trimethylammonium-propane), DOPC, and DOPG (1,2-dioleoyl-*sn*-glycero-3-phospho-(1′-*rac*-glycerol)) interacted with lipoproteins, immunoglobulins, coagulation, acute phase proteins, and complement components when exposed to human plasma. In other types of nanomaterials, such as superparamagnetic iron oxide (SPIO), the most abundant protein on the surface plasma coating was determined as C3[25], followed by serum albumin, immunoglobulin heavy constant mu, and others. Consistently, C3 was determined as the most abundant constituent of PC in our study. The PC of NPs exhibit significant variations despite sharing common components whereas NPs possessing different shell materials may manifest analogous surface PC. These inconsistencies could be attributed to a range of factors, such as particle size, composition, ZP, and fabrication techniques employed.

The surface of NPs attracts numerous proteins. The most frequently identified constituents of the corona are serum albumin, apolipoproteins, complement system proteins, immunoglobulins, and alpha-2 macroglobulin[38,39]. Several studies have demonstrated that the attachment of blood proteins to nanomaterial surfaces is a competitive adsorption process[40], while others suggest that proteins bind or adsorb NPs through stronger chemical or hydrogen bonds[41]. The proteins facilitating recognition and clearance of NPs by the IIS are yet to be clarified. The cleavage of C3 by C3-convertases is a fundamental reaction in all three complement pathways, generating two biologically active components: C3a, an anaphylatoxin; and C3b, a powerful opsonin. C3b can covalently attach to the activated surface of NPs, thereby enhancing their recognition and phagocytosis by the MPS[42]. Our research showed that the complement component covering lp-NDs contributes to phagocytosis. Data obtained by our group were concordant with other published studies. Scieszka et al.[43] reported that human polymorphonuclear neutrophils reduced uptake of liposomes when exposed to heat-inactivated-complement serum compared to normal serum. Meanwhile, Huong and colleagues observed that anti-C3 antibody treatment of serum completely blocked liposome uptake by rat peritoneal macrophages, indicating that complement receptor-mediated phagocytosis may serve as a potential mechanism for liposome uptake[44]. Subsequently, Scieszka et al.[45] showed that phagocytosis was not possible in the absence of C3 in the serum. Furthermore, they found that an antibody targeting the receptor for C3bi prevented phagocytosis in serum[45]. Klapper et al.[46] further investigated complement activation triggered by phospholipid vesicles in plasma and whole blood of humans. They reported that exposing phospholipid vesicles to plasma resulted in the production of fluid-phase complement products: C3a and SC5b-9, and granulocytes bound to or engulfed the vesicles in a manner that relied on complement activation[46]. The complement system is a complex, highly orchestrated cascade process involving multiple components. Several of the components promote phagocytosis, such as initiator complement components (C1q), membrane-binding components (C3b and C4b)[47], and complement receptor proteins (CR1 and CR3)[48]. However, the possibility that macrophages recognize lp-NDs *via* other signal transmission and receptor pathways cannot be discounted.

Ginseng (the root of *P. ginseng* C.A. Meyer, Araliaceae) is commonly used as a tonic in traditional oriental medicine[49]. The primary active component of *P. ginseng* is Gs, which has numerous beneficial pharmacological properties including antioxidant, anti-inflammatory, and immunostimulatory activities[50]. Lee et al.[51] reported inhibitory effects of four Gs (Rk3, Rh4, Rg6, and F4) on complement activation *via* the CP. The group of Kim showed strong anti-complementary activity of the total saponin fraction of *P. ginseng* against the CP but not AP at concentrations of 50−500 μg/mL[21]. So far, more than 100 types of Gs have been isolated[52]. While several researchers have reported anti-inflammatory effects of Gs Rd and Rh2[53−56], their potential anti-complement effects are yet to be established. The activities of Gs Rd and Rh2 were examined using the anti-complement hemolysis assay based on the complement fixation test as described in earlier reports[26,27]. Gs Rd and Rh2 were found to have no impact on the CP, but they were effective in inhibiting the AP. Our results were inconsistent with those of Kim et al. [21], which could be attributed to two possible factors. Firstly, Kim and co-workers investigated the anti-complementary activities against CP and AP of the total saponin fraction. Since their data indicated no anti-complementary activity against the AP of saponins, the group did not conduct further studies on the potential effects of Gs monomers against the AP. In general, the components of ginseng are distinct based on the *Panax* species, growth environment, cultivation and extraction methods[57]. Accordingly, we hypothesize that the inhibitory effect of total saponin on the AP observed in one study may not be an accurate representation of Gs monomer activity. We further modified the anti-complement assay in which the guinea pig serum or human serum was titrated to obtain submaximal levels for avoiding excess or deficiency of hemolysis (Supporting Information Materials S1 and S2). However, the lipophilic steroid structure of Gs Rd and Rh2 leads to poor water solubility, resulting in a maximum anti-complement ability of only 40%−50% even at high Gs concentrations (1 mg/mL).

Gs are natural plant-derived compounds featuring a steroid structure akin to cholesterol and have limited bioavailability due to their low water solubility[58]. This property poses a significant drawback to their therapeutic potential. Consequently, investigators have redirected their attention to the interplay between Gs and diverse phospholipids and focused on uncovering their capacity to stabilize

Please cite this article as: Zhou Jie et al., Ginsenoside modified lipid-coated perfluorocarbon nanodroplets: A novel approach to reduce complement protein adsorption and prolong *in vivo* circulation, Acta Pharmaceutica Sinica B, https://doi.org/10.1016/j.apsb.2023.11.016

the phospholipid membrane, akin to cholesterol[20,59]. The additional glycoside chain present in Gs distinguishes them from cholesterol and alters their physical and chemical characteristics[23]. The addition of the glycoside chain enhances the hydrophilic properties of Gs, which could underlie their utility as an ideal stabilizer[59]. Selvaraj et al.[60] demonstrated that the amount of released curcumin from curcumin-loaded Gs liposome is proportional to that of Gs. The group speculated that excess Gs induces a drastic shift in the hydrophilic and hydrophobic balance of the membrane. To date, numerous reports have demonstrated that encapsulation of NPs by Gs-modified phospholipids prolongs metabolic cycling and reduces clearance levels[23,61−63]. However, the precise mechanisms underlying this effect remain elusive and require further investigation. Existing research maintains that these properties are conferred by the membrane stabilization effects of Gs. However, we believe that the anti-complement effect of Gs also plays a part, along with other existing complex mechanisms that are yet to be uncovered. Simultaneously, we posit that, as indicated by Hong et al.[61], the different Gs and their distinct sugar chain structures confer disparate and intriguing effects upon anchoring. Specifically, in Hong et al.[61] investigation, when Rh2 is anchored in the liposome membrane, it exhibits an effect greater than the sum of its parts ($1 + 1 > 2$), by bolstering the stability of the lipid membrane, extending the substance's circulation duration within the bloodstream, amplifying its accumulation within tumor tissues, and prepossessing immunosuppression counteracting capabilities. Given the global magnitude of cancer as a critical public health issue and its standing as the second most prevalent cause of mortality on a global scale, the integration of Gs Rd and Rh2 as surface modifiers in lp-NDs presents a compelling prospect as an exceptionally promising and innovative drug delivery system.

An intriguing discovery from our study reveals that lp-NDs, despite our initial objective of demonstrating intracellular localization, exhibit partial co-localization with lysosomes (Fig. 2E, 6F and 6I). The escape of nanomedicine drugs from lysosomes poses a significant challenge at the intracellular level. In accordance with existing literature, it has been documented that phospholipid-based nanocarriers display higher level of co-localization with lysosomes[64]. Lysosome localization presents both advantageous and disadvantageous aspects. On the positive side, it enables passive targeting of the lysosomes. Conversely, on the negative side, this localization may lead to reduced efficacy. Our study offers evidence supporting two key findings. Firstly, it confirms the presence of lp-NDs within cells. Secondly, it demonstrates that lp-NDs exhibit a higher degree of co-localization with the lysosomal compartment, particularly in Thp-1 cell lines compared to PBMs. Meanwhile, Gs lp-NDs exhibited prolonged circulation time compared to the control group, with a longer half-life and delayed peak concentration in major MPS organs, both at the tissue cellular and macrophage levels. Although the concentration of Gs lp-NDs in the spleen appeared comparable and even higher than the control group in gross spleen fluorescence imaging, spleen homogenate, and spleen immunofluorescence sections, this might be attributed to the rapid accumulation of excessive C lp-NDs in the lungs after injection, resulting in decreased concentration in circulation. Additionally, the small size of the rat spleen may contribute to the overall reduction in the total amount of C lp-NDs entering the spleen. In larger organs such as the lungs and liver, the TFI/weight (/g) of lp-NDs was approximately 4−10 times higher than in the spleen. It was observed that Gs lp-NDs exhibited varying degrees of delayed peak concentration and lower peak intensity. However, it is important to note that using fluorescence-based methods to measure drug metabolism and distribution is only a preliminary experiment. The optimal approach would involve using nuclide labeling with DPPC.

5. Conclusions

In summary, we created a novel lp-ND system modified with Gs to address the limitations of current lp-ND formulations, including (1) non-specific clearance by the IIS (including opsonization by PC, complement system activation, and macrophage phagocytosis) and (2) short cycle times. Lp-NDs serve as ideal nanocarriers, necessitate prolonged half-life times in the bloodstream and elevated rates of delivery to the intended target site. Combinations of Gs and phospholipid exhibit multiple functionalities, including, but not limited to, inhibition of complement components and anti-phagocytosis effects. The Gs Rd and Rh2, chosen for lp-NDs modification in this research, exhibited effective anti-complement and anti-phagocytosis activities, albeit limited. Further research is warranted to identify further valuable bioactive compounds within the treasure trove of the plant kingdom.

Acknowledgments

Thank Xin Li, Yi Zhong, Tao Su and Shisheng Wang (West China Washington Mitochondria and Metabolism Research Center, West China Hospital, Sichuan University) for relative MS data acquisition and analysis. We sincerely appreciate Yan Wang, Hongying Chen and Cong Li from the Core Facilities, West China Hospital of Sichuan University for their assistance and guidance. This work was supported by the National Natural Science Foundation for Young Scholars of China (82302199), the National Science Foundation of China (82371977, 82071940) and the Medical Research Project of Chengdu Municipal Health Commission (2021017, 2022338, China).

Author contributions

Yan Luo and Feng Yan spearheaded this study by conceptualizing and designing the research, as well as revising the manuscript. Jie Zhou conducted the field trials with invaluable assistance from Binyang Gao, Huan Zhang, Rui Yang, Jianbo Huang, Yan Wang and Xiaoxia Zhu. Xin Li and Yi Zhong were responsible for performing the UPLC and LC−MS experimentation. Jie Zhou took the lead in writing the manuscript, while all authors contributed to the revision of the manuscript, ensuring its accuracy and scientific integrity. The contributions made by each author were integral to the successful execution and completion of this research study, highlighting the collaborative nature of scientific research.

Conflicts of interest

The authors have no conflicts of interest to declare.

Appendix A. Supporting information

Supporting data to this article can be found online at https://doi.org/10.1016/j.apsb.2023.11.016.

References

1. Sheng D, Liu T, Deng L, Zhang L, Li X, Xu J, et al. Perfluorooctyl bromide & Active Ingredient green co-loaded nanoliposomes for enhanced multimodal imaging-guided phototherapy. *Biomaterials* 2018;**165**: 1−13.
2. Chattaraj R, Blum NT, Goodwin AP. Design and application of stimulus-responsive droplets and bubbles stabilized by phospholipid monolayers. *Curr Opin Colloid Interface Sci* 2019;**40**:14−24.
3. Lee HY, Kim HW, Lee JH, Oh SH. Controlling oxygen release from hollow microparticles for prolonged cell survival under hypoxic environment. *Biomaterials* 2015;**53**:583−91.
4. Kaneda MM, Caruthers S, Lanza GM, Wickline SA. Perfluorocarbon nanoemulsions for quantitative molecular imaging and targeted therapeutics. *Ann Biomed Eng* 2009;**37**:1922−33.
5. La-Beck NM, Gabizon AA. Nanoparticle interactions with the immune system: clinical implications for liposome-based cancer chemotherapy. *Front Immunol* 2017;**8**:416.
6. Xiang S, Tong H, Shi Q, Fernandes JC, Jin T, Dai K, et al. Uptake mechanisms of non-viral gene delivery. *J Contr Release* 2012;**158**: 371−8.
7. Wilhelm S, Tavares AJ, Dai Q, Ohta S, Audet J, Dvorak HF, et al. Analysis of nanoparticle delivery to tumours. *Nat Rev Mater* 2016;**1**: 16014.
8. Alexis F, Pridgen E, Molnar LK, Farokhzad OC. Factors affecting the clearance and biodistribution of polymeric nanoparticles. *Mol Pharm* 2008;**5**:505−15.
9. Mcneil SE. Nanoparticle therapeutics: a personal perspective. *Wiley Interdiscip Rev Nanomed Nanobiotechnol* 2009;**1**:264−71.
10. Bazile D, Prud'Homme C, Bassoullet MT, Marlard M, Spenlehauer G, Veillard M, et al. PEG-PLA nanoparticles avoid uptake by the mononuclear phagocytes system. *J Pharmaceut Sci* 1995;**84**:493−8.
11. Perry JL, Reuter KG, Kai MP, Herlihy KP, Jones SW, Luft JC, et al. PEGylated PRINT nanoparticles: the impact of PEG density on protein binding, macrophage association, biodistribution, and pharmacokinetics. *Nano Lett* 2012;**12**:5304−10.
12. Mortimer GM, Butcher NJ, Musumeci AW, Deng ZJ, Martin DJ, Minchin RF. Cryptic epitopes of albumin determine mononuclear phagocyte system clearance of nanomaterials. *ACS Nano* 2014;**8**: 3357−66.
13. Chen E, Chen B, Su Y, Chang Y, Cheng T, Barenholz Y, et al. Premature drug release from polyethylene glycol (PEG)-coated liposomal Active Ingredient *via* formation of the membrane attack complex. *ACS Nano* 2020;**14**:7808−22.
14. Shi J, Kantoff PW, Wooster R, Farokhzad OC. Cancer nanomedicine: progress, challenges and opportunities. *Nat Rev Cancer* 2017;**17**: 20−37.
15. Mohamed M, Abu LA, Shimizu T, Alaaeldin E, Hussein A, Sarhan HA, et al. PEGylated liposomes: immunological responses. *Sci Technol Adv Mater* 2019;**20**:710−24.
16. Walport MJ. Complement. First of two parts. *N Engl J Med* 2001;**344**: 1058−66.
17. Kugelberg E, Gollan B, Tang CM. Mechanisms in Neisseria meningitidis for resistance against complement-mediated killing. *Vaccine* 2008;**26**(Suppl 8):I34−9.
18. Lee MH, Lee BH, Jung JY, Cheon DS, Kim KT, Choi C. Antiviral effect of Korean red ginseng extract and ginsenosides on murine norovirus and feline calicivirus as surrogates for human norovirus. *J Ginseng Res* 2011;**35**:429−35.
19. Shibata S, Fujita M, Itokawa H, Tanaka O, Ishii T. Studies on the constituents of Japanese and Chinese crude drugs. Xi. Panaxadiol, a sapogenin of ginseng roots. *Chem Pharm Bull (Tokyo)* 1963;**11**: 759−61.
20. Wang H, Zheng Y, Sun Q, Zhang Z, Zhao M, Peng C, et al. Ginsenosides emerging as both bifunctional drugs and nano-carriers for enhanced antitumor therapies. *J Nanobiotechnol* 2021; **19**:322.
21. Kim DS, Oh SR, Lee IS, Jung KY, Park JD, Kim SI, et al. Anti-complementary activity of ginseng saponins and their degradation products. *Phytochemistry* 1998;**47**:397−9.
22. Xia J, Ma S, Zhu X, Chen C, Zhang R, Cao Z, et al. Versatile ginsenoside Rg3 liposomes inhibit tumor metastasis by capturing circulating tumor cells and destroying metastatic niches. *Sci Adv* 2022;**8**:eabj1262.
23. Hong C, Wang D, Liang J, Guo Y, Zhu Y, Xia J, et al. Novel ginsenoside-based multifunctional liposomal delivery system for combination therapy of gastric cancer. *Theranostics* 2019;**9**:4437−49.
24. Tenzer S, Docter D, Kuharev J, Musyanovych A, Fetz V, Hecht R, et al. Rapid formation of plasma protein corona critically affects nanoparticle pathophysiology. *Nat Nanotechnol* 2013;**8**:772−81.
25. Vu VP, Gifford GB, Chen F, Benasutti H, Wang G, Groman EV, et al. Immunoglobulin deposition on biomolecule corona determines complement opsonization efficiency of preclinical and clinical nanoparticles. *Nat Nanotechnol* 2019;**14**:260−8.
26. Oh SR, Ryu SY, Park SH, Jung KY, Lee IS, An KS, et al. Anti-complementary activity of stilbenes from medicinal plants. *Arch Pharm Res (Seoul)* 1998;**21**:703−6.
27. Klerx JPAM, Beukelman CJ, Van Dijk H, Willers JMN. Microassay for colorimetric estimation of complement activity in Guinea pig, human and mouse serum. *J Immunol Methods* 1983;**63**:215−20.
28. Yang ST, Luo J, Zhou Q, Wang H. Pharmacokinetics, metabolism and toxicity of carbon nanotubes for biomedical purposes. *Theranostics* 2012;**2**:271−82.
29. Willmann JK, Cheng Z, Davis C, Lutz AM, Schipper ML, Nielsen CH, et al. Targeted microbubbles for imaging tumor angiogenesis: assessment of whole-body biodistribution with dynamic micro-PET in mice. *Radiology* 2008;**249**:212−9.
30. van Meer G, Voelker DR, Feigenson GW. Membrane lipids: where they are and how they behave. *Nat Rev Mol Cell Biol* 2008;**9**:112−24.
31. Cai W, Chen X. Nanoplatforms for targeted molecular imaging in living subjects. *Small* 2007;**3**:1840−54.
32. Das SK, Sarkar S, Dash R, Dent P, Wang XY, Sarkar D, et al. Chapter One—Cancer terminator viruses and approaches for enhancing therapeutic outcomes. *Adv Cancer Res* 2012;**115**:1−38.
33. Dash R, Azab B, Shen XN, Sokhi UK, Sarkar S, Su ZZ, et al. Developing an effective gene therapy for prostate cancer: new technologies with potential to translate from the laboratory into the clinic. *Discov Med* 2011;**11**:46−56.
34. Evans DR, Parsons DF, Craig VS. Physical properties of phase-change emulsions. *Langmuir* 2006;**22**:9538−45.
35. Mitragotri S, Lahann J. Physical approaches to biomaterial design. *Nat Mater* 2009;**8**:15−23.
36. Corbo C, Molinaro R, Taraballi F, Toledano FN, Sherman MB, Parodi A, et al. Effects of the protein corona on liposome-liposome and liposome-cell interactions. *Int J Nanomed* 2016;**11**:3049−63.
37. Giulimondi F, Digiacomo L, Pozzi D, Palchetti S, Vulpis E, Capriotti AL, et al. Interplay of protein corona and immune cells controls blood residency of liposomes. *Nat Commun* 2019;**10**:3686.
38. Walkey CD, Chan WC. Understanding and controlling the interaction of nanomaterials with proteins in a physiological environment. *Chem Soc Rev* 2012;**41**:2780−99.
39. Shannahan JH, Brown JM, Chen R, Ke PC, Lai X, Mitra S, et al. Comparison of nanotube-protein corona composition in cell culture media. *Small* 2013;**9**:2171−81.
40. Onishchenko N, Tretiakova D, Vodovozova E. Spotlight on the protein corona of liposomes. *Acta Biomater* 2021;**134**:57−78.
41. Piloni A, Wong CK, Chen F, Lord M, Walther A, Stenzel MH. Surface roughness influences the protein corona formation of glycosylated nanoparticles and alter their cellular uptake. *Nanoscale* 2019;**11**: 23259−67.
42. Regal JF, Burwick RM, Fleming SD. The complement system and preeclampsia. *Curr Hypertens Rep* 2017;**19**:87.
43. Scieszka JF, Cho MJ. Cellular uptake of a fluid-phase marker by human neutrophils from solutions and liposomes. *Pharm Res (N Y)* 1988;**5**:352−8.

Please cite this article as: Zhou Jie et al., Ginsenoside modified lipid-coated perfluorocarbon nanodroplets: A novel approach to reduce complement protein adsorption and prolong *in vivo* circulation, Acta Pharmaceutica Sinica B, https://doi.org/10.1016/j.apsb.2023.11.016

44. Huong TM, Harashima H, Kiwada H. Complement dependent and independent liposome uptake by peritoneal macrophages: cholesterol content dependency. *Biol Pharm Bull* 1998;**21**:969−73.
45. Scieszka JF, Maggiora LL, Wright SD, Cho MJ. Role of complements C3 and C5 in the phagocytosis of liposomes by human neutrophils. *Pharm Res (N Y)* 1991;**8**:65−9.
46. Klapper Y, Hamad OA, Teramura Y, Leneweit G, Nienhaus GU, Ricklin D, et al. Mediation of a non-proteolytic activation of complement component C3 by phospholipid vesicles. *Biomaterials* 2014;**35**:3688−96.
47. Talaat IM, Elemam NM, Saber-Ayad M. Complement system: an immunotherapy target in colorectal cancer. *Front Immunol* 2022;**13**:810993.
48. Qin X, Gao B. The complement system in liver diseases. *Cell Mol Immunol* 2006;**3**:333−40.
49. Lee JH, Ahn JY, Shin TJ, Choi SH, Lee BH, Hwang SH, et al. Effects of minor ginsenosides, ginsenoside metabolites, and ginsenoside epimers on the growth of Caenorhabditis elegans. *J Ginseng Res* 2011;**35**:375−83.
50. Kim SK, Park JH. Trends in ginseng research in 2010. *J Ginseng Res* 2011;**35**:389−98.
51. Lee JG, Baek SH, Lee YY, Park SY, Park JH, Acollege OPAR, et al. Anti-complementary ginsenosides isolated from processed ginseng. *Biol Pharm Bull* 2011;**34**:898−900.
52. Shin BK, Kwon SW, Park JH. Chemical diversity of ginseng saponins from *Panax ginseng*. *J Ginseng Res* 2015;**39**:287−98.
53. Yi PF, Bi WY, Shen HQ, Wei Q, Zhang LY, Dong HB, et al. Inhibitory effects of sulfated 20(S)-ginsenoside Rh2 on the release of pro-inflammatory mediators in LPS-induced RAW 264.7 cells. *Eur J Pharmacol* 2013;**712**:60−6.
54. Bi WY, Fu BD, Shen HQ, Wei Q, Zhang C, Song Z, et al. Sulfated derivative of 20(S)-ginsenoside Rh2 inhibits inflammatory cytokines through MAPKs and NF-kappa B pathways in LPS-induced RAW264.7 macrophages. *Inflammation* 2012;**35**:1659−68.
55. Tang K, Qin W, Wei R, Jiang Y, Fan L, Wang Z, et al. Ginsenoside Rd ameliorates high glucose-induced retinal endothelial injury through AMPK-STRT1 interdependence. *Pharmacol Res* 2022;**179**:106123.
56. Mathiyalagan R, Wang C, Kim YJ, Castro-Aceituno V, Ahn S, Subramaniyam S, et al. Preparation of polyethylene glycol-ginsenoside rh1 and rh2 conjugates and their efficacy against lung cancer and inflammation. *Molecules* 2019;**24**:4367.
57. Jia L, Zhao Y, Liang XJ. Current evaluation of the millennium phytomedicine- ginseng (II): collected chemical entities, modern pharmacology, and clinical applications emanated from traditional Chinese medicine. *Curr Med Chem* 2009;**16**:2924−42.
58. Antao AR, Bangay G, Dominguez-Martin EM, Diaz-Lanza AM, Rijo P. *Plectranthus ecklonii* benth: a comprehensive review into its phytochemistry and exerted biological activities. *Front Pharmacol* 2021;**12**:768268.
59. Wang MZ, Xu Y, Xie JF, Jiang ZH, Peng LH. Ginsenoside as a new stabilizer enhances the transfection efficiency and biocompatibility of cationic liposome. *Biomater Sci* 2021;**9**:8373−85.
60. Selvaraj K, Yoo BK. Curcumin-Loaded nanostructured lipid carrier modified with partially hydrolyzed ginsenoside. *AAPS PharmSciTech* 2019;**20**:252.
61. Hong C, Liang J, Xia J, Zhu Y, Guo Y, Wang A, et al. One stone four birds: a novel liposomal delivery system multi-functionalized with ginsenoside rh2 for tumor targeting therapy. *Nano-Micro Lett* 2020;**12**:129.
62. Singh P, Kim YJ, Singh H, Ahn S, Castro-Aceituno V, Yang DC. *In situ* preparation of water-soluble ginsenoside Rh2-entrapped bovine serum albumin nanoparticles: *in vitro* cytocompatibility studies. *Int J Nanomed* 2017;**12**:4073−84.
63. Xia X, Tao J, Ji Z, Long C, Hu Y, Zhao Z. Increased antitumor efficacy of ginsenoside Rh2 *via* mixed micelles: *in vivo* and *in vitro* evaluation. *Drug Deliv* 2020;**27**:1369−77.
64. Veeren A, Ogunyankin MO, Shin JE, Zasadzinski JA. Liposome-tethered gold nanoparticles triggered by pulsed NIR light for rapid liposome contents release and endosome escape. *Pharmaceutics* 2022;**14**:701.

Please cite this article as: Zhou Jie et al., Ginsenoside modified lipid-coated perfluorocarbon nanodroplets: A novel approach to reduce complement protein adsorption and prolong *in vivo* circulation, Acta Pharmaceutica Sinica B, https://doi.org/10.1016/j.apsb.2023.11.016